EXPLORING CHEMICALLY TREATED FIBER REINFORCED PERVIOUS CONCRETE THROUGH IMAGE BASED MICROMECHANICAL MODELING

A Dissertation
Submitted to the Graduate Faculty
of the
North Dakota State University
of Agriculture of Applied Science

By

Lutfur Rahman Akand

In Partial Fulfillment of the Requirements
for the Degree of
DOCTOR OF PHILOSOPHY

Major Department:
Civil and Environmental Engineering

April 2019

Fargo, North Dakota

North Dakota State University

Graduate School

Title

EXPLORING CHEMICALLY TREATED FIBER REINFORCED PERVIOUS CONCRETE THROUGH IMAGE BASED MICROMECHANICAL MODELING

By

Lutfur Rahman Akand

The Supervisory Committee certifies that this disquisition complies with North Dakota State University's regulations and meets the accepted standards for the degree of

DOCTOR OF PHILOSOPHY

SUPERVISORY COMMITTEE:

Dr. Mijia Yang
Chair

Dr. Ghodrat Karami

Dr. Kalpana Katti

Dr. Jerry Gao

Dr. Xinnan Wang

Approved:

11/14/2019
Date

Dr. David R. Steward
Department Chair

ABSTRACT

Pervious concrete has been widely used in parking lots and airport fields. However, past experience has shown durability and strength of the pervious concrete remains a challenge for adopting them in wider applications, as the binding material proportion is low and the use of fine aggregates is nearly zero. The position, size and shape distribution of voids in the pervious concrete microstructure control the overall behavior of the material. In this research, the influence of the distribution of voids on the strength, stiffness, and permeability of pervious concrete microstructure is studied by 2D image analysis and finite element modeling through MATLAB and ANSYS Parametric Design Language (APDL). The effect of the sample size of 2D microstructures is studied by varying the section size and a possible representative volume element (RVE) is therefore found. Predicted stress-strain plots are generated for the 2D specimen under compressive load and the obtained results, including stiffness, strength and permeability are compared with the results from the experiments conducted following ASTM standards.

In order to enhance bonding between reinforcement fiber and cement matrix, chemical treatment is adopted and applied on short polypropylene fibers when used in pervious concrete as reinforcement. The change in fiber surface due to the treatment is determined through fiber wettability test and Atomic Force Microscopy (AFM). Single fiber pullout tests are conducted to study the effect of the treatment type on fiber-cement interface properties. Treated fibers are then put into pervious concrete matrix for compressive and flexural strength tests.

With the chemical treated fibers, 2D microstructures of fiber reinforced pervious concrete are generated and cohesive zone technique is used to model the interface between fiber and concrete matrix, with its interface properties extracted from single fiber pullout tests. Load-displacement plots are generated in ANSYS for specimen under compression for different mixes.

Through the validated micromechanical model and its modeling results of different fiber reinforced pervious concrete mix, an optimization method is developed to provide a useful tool for mix design of reinforced pervious concrete with chemically treated fibers.

ACKNOWLEDGEMENTS

First and foremost, I would like to express my sincere gratitude and appreciation to my advisor, Dr. Mijia Yang, for his continuous support and guidance during my study at NDSU. The completion of my dissertation would not have been possible without his valuable advice, encouragement and continuous support. Dr. Yang enriched my thinking process as a researcher and always guided me to right direction with his immense wisdom and knowledge. His guidance and advises will benefit my future career track and help me to reach my goals. I also want to thank all my dissertation committee members, Dr. Ghodrat Karami, Dr. Kalpana Katti, Dr. Jerry Gao and Dr. Xinnan Wang, for their suggestion and help during the course of my graduate study. I am thankful to Department of Civil and Environmental Engineering, North Dakota State University, for supporting my Doctoral study and for allowing me to work as a teaching assistant. Last, but not the least, I would like to thank my parents, my wife, my son, my sibling and all the other family members for their unconditional support and love.

DEDICATION

This dissertation is dedicated to all the good people who are working towards humanity and to make this world a better living place for the future generation.

TABLE OF CONTENTS

LIST OF TABLES

LIST OF FIGURES

LIST OF APPENDIX FIGURES

CHAPTER 1. INTRODUCTION AND LITERATURE REVIEW

1.1. History and Properties of Pervious Concrete

Pervious concrete is a special type of concrete with very little or no fine aggregate and with a substantial amount of porosity, usually varies from 15~25%. It was first introduced in Europe in early 19th century. Pervious concrete became a viable construction material in Russian Federation, Africa and Middle East during the post-World War II era as a result of cement scarcity at that time. Practice of using pervious concrete for light-weight construction started in USA in 1970's.

The mix design of pervious concrete remained a challenge since its early days. The amount of cementitious materials and water content are carefully controlled to form a thick paste of coating around the coarse aggregate, just enough to bond the aggregates together and maintain a high porosity. With very little or no sand content, the interconnected pores provide a very permeable surface and lets water drain through quickly. Typical permeability of pervious concrete is around 0.3~0.4 cm/s (480~550 in/hr), but it can vary depending on the mix design. Compared to the conventional concrete, pervious concrete has much lower compressive strength due to high porosity and low mortar content. Pervious concrete is successfully placed in drive-ways, parking lots, where the concrete structure is subjected to less traffic and requires lower load capacity.

Pervious concrete has been used for various applications worldwide and in United States. The primary application is in pavement. In pavement industry, pervious concrete is often referred as porous concrete, no-fines concrete or gap-graded concrete. Researchers around the world has been studying the properties of pervious concrete material, such as strength, porosity, freeze-thaw durability etc. to produce a pavement material that is durable and less susceptible to failure. Enhancements such as admixture and fibers have been used and lab experiments have been carried out.

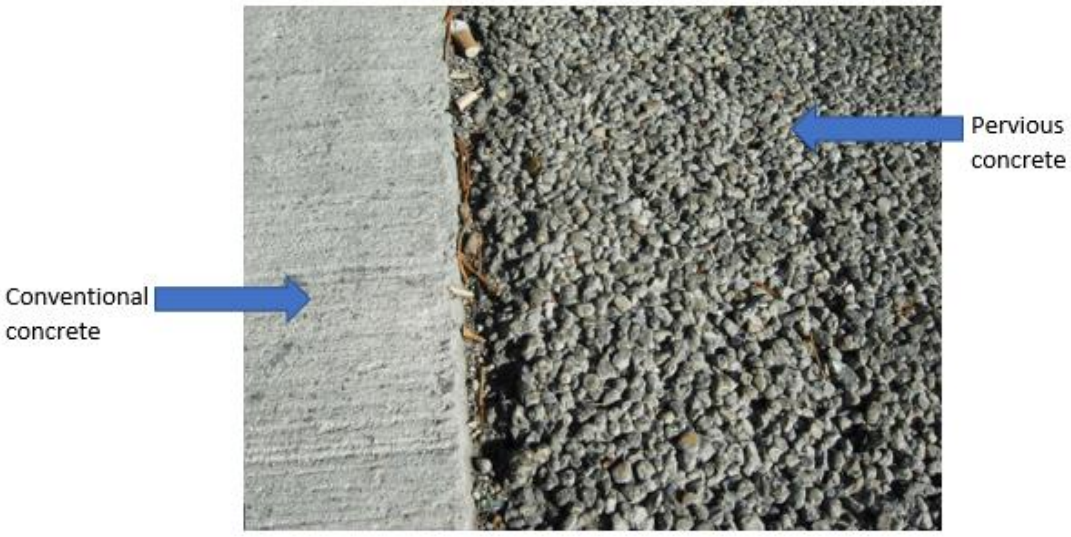

Fig. 1.1. Side by side visual comparison of conventional and pervious concrete [Source: go-gba.org]

However, the improvement in strength and durability of pervious concrete is limited and remains a challenge till date.

1.2. Benefits of Using Pervious Concrete

Using pervious concrete is beneficial for several reasons. The major advantage is its higher permeability than that of conventional concrete. Due to high porosity, pervious concrete has lower unit weight and higher thermal insulation values.

The leading priority of using pervious concrete is due to ensure better stormwater management. U.S. Environmental Protection Agency has declared pervious concrete as one of the best management practices for surface runoff and stormwater drainage. Pervious concrete acts as a filter to prevent pollutants to reach the groundwater. Major sources of surface pollutants that come through urban runoff are heavy metals (from dripping vehicles and exhausts), sediment in forms of dirt and debris, hydrocarbon from vehicles and binder and sealer used in asphalt pavement. EPA shows that almost 90 percent of these pollutants are carried though the surface runoff due to rain and run into the natural water bodies. Urban stormwater drainage system

generally carries these pollutants to rivers, lakes, ponds. As a result, water sources don't remain potable and the aquatic life is severely affected. Use of asphalt in pavement also possesses a threat to a green environment, as asphalt is the major source of chemical pollutants such as hydrocarbons.

Pervious concrete pavement that uses less asphalt and prevents surface pollutants getting into groundwater is becoming the most feasible solution to these issues, which includes

- Infiltrates storm runoff and reduces the untreated water discharge to the storm sewer system
- Recharge the groundwater level directly through filtered rainfall.
- Reduces the need of irrigation system by channeling water to the landscape and tree roots.
- Filter pollutants and mitigate the risk of contaminants reaching the watersheds.
- Eliminate the hydrocarbon pollution.

Besides stormwater management, pervious concrete can reduce the 'heat island' effect, an effect that occurs due to excessive heat generation due to concrete infrastructure. Pervious concrete is light colored, and its high porosity induces a cellular structure, which makes it absorbs and stores less heat than conventional concrete or asphalt pavement does. Pervious pavement remains cooler as it allows air circulation.

From safety standpoint, pervious concrete is safer for drivers and pedestrians. As no water can stand on it and drains quickly, pervious concrete is not prone to puddling, icing, hydroplaning etc. Pervious concrete pavement surface offers a good roughness and grip to vehicle tires and pedestrians as well.

1.3. Common Problems with Pervious Concrete

The use of pervious concrete is limited to certain areas such as low traffic, low load-bearing zones. When choosing pervious concrete as a pavement alternative, designers face some challenges. Pervious concrete provides lower compressive and flexural strength than conventional concrete does as the bond strength is low between adjacent coarse aggregates. Pervious concrete is prone to clogging. Its permeability can be significantly reduced for that. Some other disadvantages of pervious concrete usage could be listed as:

- Compared to conventional concrete, pervious concrete is expensive to install. Its mix design needs more attention and other factors like runoff characteristics, type of debris or sediment etc. need to be considered.
- Pervious concrete needs regular maintenance as it could get clogged. Excessive dirt, debris, plant substances can get into the void spaces and block the pores. The clogging disrupts the purpose of pervious concrete, draining stormwater runoff and filtering pollutants. Clogged pores can be subjected to swell and spall and hence reduce the lifetime of the pavement.
- Low compressive strength is a major concern and limits the use of pervious concrete in regular roadways that carry traffic flow and are subjected to impact loads. Due to its porous structure, cracks can propagate quickly in pervious concrete, and lead to spalling or potholes in pavement.

1.4. Current Research

Pervious concrete has been used for over 30 years and researchers are conducting both laboratory experiments and numerical modeling to achieve a sustainable material. To maintain high void ratio and permeability, pervious concrete mix design demands a careful attention on choosing cement and coarse aggregate proportion. Studies have shown that an addition of a very little fine aggregate can improve the strength of pervious concrete. Researchers have studied a wide range of mix proportions to reach to a sustainable mix design of pervious concrete. Typical composition of pervious concrete is tabulated in Table 1.1.

Porosity is one of the most important parameters to consider while conducting pervious concrete mix design. However, there is still confusion regarding the definition of porosity and the type of porosity that should be used to characterize pervious concrete. Not all voids in PC are effective for liquids to flow through. Zhong et al. (2015) suggested that the pore system in pervious concrete should be differentiated as effective porosity and total porosity. Effective porosity is defined as the ratio of the volume of connected pores to the total volume of the material; while total porosity is defined as the ratio of total pore volume to the total volume of material. Effective porosity controls the hydraulic properties of pervious concrete, while total porosity dictates its strength.

Table 1.1. Typical mix proportions of pervious concrete

Water-Cement ratio	Aggregate-Cement ratio	Fine aggregate (sand) %	Authors
0.26 – 0.33	3.2 – 3.7	0 - 15	Kevern et al. (2011)
0.32 – 0.33	1.7 – 6.0	-	Deo et al. (2011)
0.22 – 0.55	2.5 – 3.5	-	Zhong et al. (2015)
0.25 – 0.35	3.2 – 3.9	-	Yang et al. (2011)
0.37 – 0.42	2.9 – 4.2	-	Ghaffori et al. (1995)
0.27 – 0.35	3.4 – 4.5	0 – 6.5	Huang et al. (2010)
0.27 – 0.51	4.0 – 4.7	0 - 20	Meininger et al. (1988)

Different techniques could be used to determine the porosity of pervious concrete such as laboratory experiments and image analysis techniques. Statistical determination of porosity using image analysis (IA) and statistical counts has been proposed by Zhong et al. (2015) to quantify the porosity of pervious concrete. In this study, 16-bit greyscale X-ray planar images of a series of pervious concrete thin sections were employed. A similar image analysis approach was also employed by Neithalath et al. (2010) and Marolf et al. (2004) to quantify porosity. Different facilities such as X-ray computed tomography and flatbed scanner have been used to obtain the original images.

Pore size distribution in pervious concrete specimen has been studied by researchers to characterize the matrix. Deo et al. (2011) found that the compressive response of pervious concrete is influenced by its pore sizes, their distributions and spacing. Zhong et al. (2016) also confirmed the influence of pore size and its distribution on the compressive strength of pervious concrete. Rehder et al. (2014) demonstrated that the fracture toughness is primarily dependent on the

porosity of pervious concrete and an increase in pore size leads to a reduction in fracture toughness at a given porosity.

As strength and durability remain as issues for using pervious concrete, researchers also put attention to enhance the mechanical properties by adding admixtures and fibers. numerous improvements have been introduced to the PC mixture design to address the above-stated objectives. Hesami et al. (2014) focused on improving the mechanical properties by inclusion of rice husk fibers. Rehder et al. (2014) reported that polypropylene fibers introduced improvements in residual flexural strength of pervious concrete. Kevern et al. (2008) added liquid admixtures while mixing the cement and coarse aggregate and achieved considerable improvement on the compressive strength. Amde et al. (2013) considered using polypropylene and fiberglass fibers and reported the enhancement of compressive strength and durability of pervious concrete specimen.

1.5. Scope of The Study

Pervious concrete has huge potential to be used as an environment friendly alternative solution to conventional concrete and asphalt pavement. Understanding its pore geometry at micro level could help better understanding of the behavior of pervious concrete matrix, including its failure under loading. As laboratory experiments are expensive and time consuming, finding a representative pervious concrete microstructure that represents the entire specimen and studying the mechanical properties of pervious concrete through that microstructure can be a feasible alternative.

Use of fiber in pervious concrete raises a question mark, as the use of cementitious material is low and the contact area between fiber and the concrete matrix is limited. Researchers have tried different fibers to enhance the compressive and flexural strength of the matrix. However,

enhancing the fiber surface properties by chemical or mechanical treatment to increase the bond strength between fiber and concrete matrix can be a convenient technique. If a significant improvement can be reached on enhancing the bond strength between fiber and concrete matrix interface, the crack growth and propagation can be delayed and hence the mechanical properties of pervious concrete will be increased.

The implementation of fiber-matrix interface mechanics in a porous structure like pervious concrete is a challenge. Cohesive interface model with imperfect bonding will be useful to study the characteristics of fiber-reinforced pervious concrete.

This thesis characterizes the pervious concrete through an imaged based micromechanical model, which is described in Chapter 2. Polypropylene fibers are chemically treated to enhance the surface roughness properties and then added to pervious concrete. Laboratory experiments have been conducted to prove the enhancement of fiber surface roughness and the fiber matrix bond strength, which is included in Chapter 3. Chapter 4 studied fiber-matrix interface properties extracted from single fiber pullout tests. A 2D fiber reinforced pervious concrete model is generated with the fiber-matrix interface properties based on cohesive zone model. Finally, Chapter 5 proposed a statistical approach to optimize the fiber reinforced pervious concrete which could provide a useful tool for mix designs of pervious concrete. Chapter 6 will summarize the conclusions and future works.

1.6. References

[1] Kevern J.T., Schaefer V.R., Wang K., (2011). Mixture proportion development and performance of pervious concrete for overlay applications, ACI Mater. J. 108 (4) 439–448.

[2] Deo O., Neithalath N., (2011). Compressive response of pervious concretes proportioned for desired porosities, Constr. Build. Mater. 25, 4181–4189.

[3] Zhong R., Wille K., (2015). Material design and characterization of high performance pervious concrete, Constr. Build. Mater. 98, 51–60.

[4] Yang Z., (2011). Freezing-and-thawing durability of pervious concrete under simulated field conditions, ACI Mater. J. 108 (2) ,187–195.

[5] Ghafoori N., Dutta S., (1995). Laboratory investigation of compacted no-fines concrete for paving materials, J. Mater. Civ. Eng. 7 (3), 183–191.

[6] Huang B., Wu H., Shu X., Burdette E.G., (2010). Laboratory investigation of permeability and strength of polymer-modified pervious concrete, Constr. Build. Mater. 24, 818–823.

[7] Meininger R.C., (1988). No-fines pervious concrete for paving, Concr. Int. 10 (8), 20–27.

[8] Zhong R., Xu M., Netto R.V., (2016). Wille K., Influence of pore tortuosity on hydraulic conductivity of pervious concrete: characterization and modeling, Constr. Build. Mater. 125, 1158–1168.

[9] Neithalath N., Sumanasooriya M.S., Deo O., (2010). Characterizing pore volume, sizes, and connectivity in pervious concretes for permeability prediction, Mater. Charact. 61, 802–813.

[10] Marolf A., Neithalath N., Sell E., Wegner K., Weiss J., Olek J., (2004). Influence of aggregate size and gradation on the acoustic absorption of enhanced porosity concrete, ACI Mater. J. 101 (1), 82–91.

[11] Zhong R., Wille K., (2016). Linking pore system characteristics to the compressive behavior of pervious concrete, Cem. Concr. Compos. 70, 130–138.

[12] Hesami S., Ahmadi S., Nematzadeh M., (2014). Effects of rice husk ash and fiber on mechanical properties of pervious concrete pavement, Constr. Build. Mater., 53, pp. 680-691.

[13] Rehder B., Banh K., Neithalath N., (2014). Fracture behavior of pervious concretes: the effects of pore structure and fibers, Eng. Fract. Mech., 118, pp. 1-16

[14] Kevern J.T., Schaefer V.R., Wang K., Suleiman M.T., (2008). Pervious concrete mixture proportions for improved freeze-thaw durability, J. ASTM Int., 5 (2), p. 12

[15] Amde A.M., Rogge S., (2013). Development of High Quality Pervious Concrete Specifications for Maryland Conditions, Final Report, MD-13-SP009B4F

CHAPTER 2. CHARACTERIZATION OF PERVIOUS CONCRETE THROUGH IMAGE BASED MICROMECHANICAL MODELING

2.1. Introduction

Due to a high percentage of porosity (10-25%), the 7-day compressive strength of typical pervious concrete is around 1500~2000 psi (10.3~13.8 MPa) (Chopra et al., 2007a), which limits its application and long-term durability. Field investigations for pervious concrete pavements have shown excessive crack generation and spalling of the concrete surface, which eventually reduces the service life of the overall pavement system (Chopra et al., 2007b). In cold weather regions, this issue is even more prominent due to the freeze-thaw cycles the pervious concrete experienced. Researchers around the world have implemented different mix designs and performed excessive experimental studies to find a sustainable pervious concrete mix (Yang et al., 2003, Kevern et al., 2008, Kevern et al., 2010). Attempts have been taken to introduce fiber to the pervious concrete, but due to lack of effective fiber-concrete interface bonding, the strength improvement remained insignificant (Made et al., 2013). In order to understand the mechanical behavior and enhance the long-term performance of pervious concrete, an image-based micromechanical model of the pervious concrete is suggested in this paper to enhance understanding of the relationship between microstructure and macro behavior of the material.

Jing Hu et al. (2003) discussed the nature of pore structure through backscattered electron (BSE) images of polished sections of cement paste material. Pore size distribution was characterized, and the critical pore size was determined for the cement paste at different hydration times. The influence of image resolution was also investigated in the study. Wong et al. (2006) presented a technique to distinguish pores from a normal backscattered electron image of cement-based material. The study described a critical point where a small incremental gray value caused

a sudden increase in porosity estimation, a condition termed as overflow. Lange et al. (1994) also explored the nature of pore structure through backscattered electron images of polished cement-based material sections.

Image analysis techniques used in this study included sizing, two-point correlation, and fractal analyses. Pore size distribution from Mercury Intrusion Porosimetry (MIP) was compared to void size distribution derived from backscattered electron images. Igarashi et al. (2009) compared the microstructure of cement pastes revealed by SEM-BSE image analysis with a simulated structure generated by the CEMHYD3D hydration simulation model developed at University of Twente. The spatial array of unhydrated cement particles was simulated by the model. However, spatial features in capillary pore structure obtained by the simulation were different from the microstructure derived on SEM-BSE images.

Pervious concrete collects pavement surface water and waste and filter them through its pore structures. Pervious concrete increases driver safety and enhance environment cleanness, which has been widely used in airport, parking lots, etc. However due to its weak weariness and strength, pervious concrete shows low durability and could not be applied to applications with high load demand. Enhancement of the strength and stiffness of the pervious concrete highly depends on the behavior of the microstructure. Based on this, the goal of this study is to propose a quick and convenient tool to characterize the porous microstructures of pervious concrete and predict its mechanical behavior through its microstructure. The chapter is divided into five sections. In section 1, position and size distribution of voids on the 2D electron microscopy image of the pervious concrete specimen are analyzed through SEM images. In section 2, a micro-structure model regenerated with the derived distribution parameters in section 1. In section 3, a FEM model is created to model the progressive failure of the pervious concrete. In section 4, the simulated

results are then compared with the lab experiments. A summary is provided in section 5 to conclude the study and opens the door for further application of the model to optimally design the pervious concrete.

2.2. Image Analysis of Pervious Concrete Specimen

2.2.1. Image Analysis through ImageJ

The void distribution inside the pervious concrete is captured through electron microscope. The sample was attached to a 100 mm square plastic petri dish using hot glue and placed into a GE Phoenix X-ray computed tomography system (MicroCT) equipped with a 180-kV high power nanofocus X-ray tube. One thousand two hundred seventy-five projections of the sample were acquired for each scan at a voltage of 140 kV and a current of 250 mA. Detector timing was set to 1000 ms and the total acquisition time was 1 hour and 6 minutes per scan. The sample magnification was 1.6x with a voxel size of 122.58 mm. For the larger sample size, 4" diameter x 8" height (ϕ 100 mm x 200 mm), the sample was divided into three separate scans. The acquired images from each scan were merged and reconstructed into a volume data set using GE datos|x 3D computer tomography software version 2.2. The reconstructed volume was then viewed and manipulated using VGStudio Max 2.2 by Volume Graphics. 2D section was taken from two different specimens with a maximum size of 94.0x68.6 mm (3.7" x 2.7", batch 1) and 200x100 mm (8.0"x4.0", batch 2) respectively. Several sections with a consistent increment ratio in sizes are taken from the full image (Fig. 2.1). These sections are then analyzed with the ''ImageJ'' software platform developed by National Institute of Health (NIH) (Collins et al. 2007).

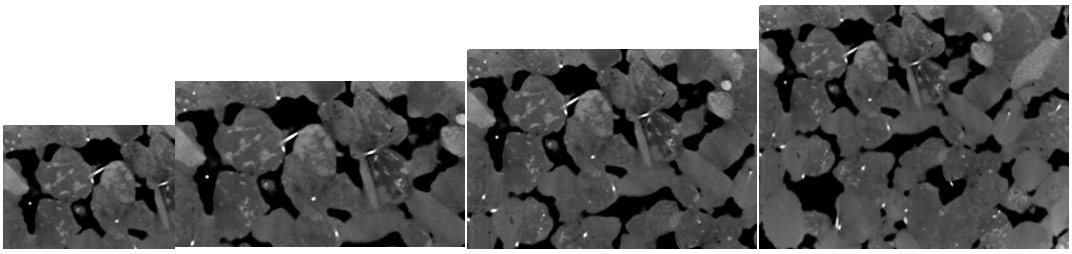

Fig. 2.1. Different section sizes from the same image

The voids are first separated from the concrete matrix through a threshold gray value of the image (Fig. 2.2(b)). The voids are then outlined in the image showing their sizes and their positions in the matrix (Fig. 2.3(c)).

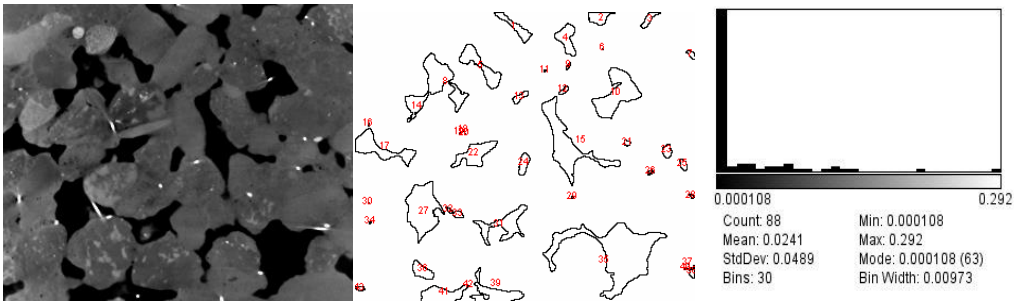

(a) (b) (c)

Fig.2.2. Void distribution by image analysis (a) microscopic image (b) voids separated from matrix (c) histogram of void size distribution

The position of each void has been located through the X and Y coordinate values of their centroid. The area of each void has been tabulated and the void percentage is then calculated from the area data. The pore size distribution is first analyzed through Fast Fourier Transformation (FFT) and the resultant distribution is then transferred to MATLAB to regenerate the pervious concrete microstructure. Different regeneration represents a virtual sampling of the pervious concrete matrix.

2.2.2. Fast Fourier Transformation (FFT) of the Void Distribution

From the image analysis data, the relative position (X and Y coordinates) of the voids for different section sizes was plotted as histograms to describe any possible pattern of the distribution. However, the plots showed that the distribution of voids through the entire section of specimen does not follow any apparent pattern with the increment of section size (Fig. 2.3). In this study, a Fast Fourier transformation (FFT) analysis is conducted on the void distribution obtained from the image analysis data and the dominant distribution frequencies are extracted.

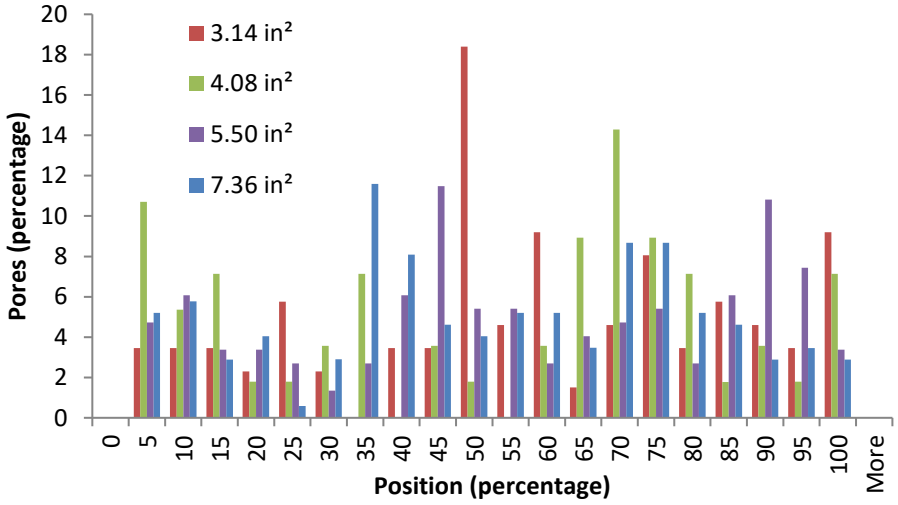

Fig. 2.3. Histogram showing percentage of pores in a certain location of the matrix (1 in. = 25 mm)

The method of adopting FFT analysis for void characterization is not totally new. Moulinec et al. (1994) adopted this method in characterizing the inhomogeneous distribution of porosity and studied its effect on the nonlinear behavior of a composite material. Nicolas Bilgar et al. (2005) performed numerical simulations on different spatial distributions of voids generated through the FFT derived distribution parameters. Three types of microstructures were investigated: random microstructures with no void clustering, microstructures with a connected cluster of voids, and microstructures with disconnected void clusters.

Using the derived statistical distribution parameter of voids, the porous microstructure is regenerated through a MATLAB code and fed to ANSYS for further analysis. The FFT distribution of voids on the actual image and the MATLAB generated microstructure is compared to confirm the accuracy of the distribution (Fig. 2.4). A close match of the void size distribution is clearly seen in Fig. 2.4. From Fig. 2.4, a major uniform distribution of void positions is observed, with a small clustering (around 5%) at locations of the 40% and 60% specimen dimension.

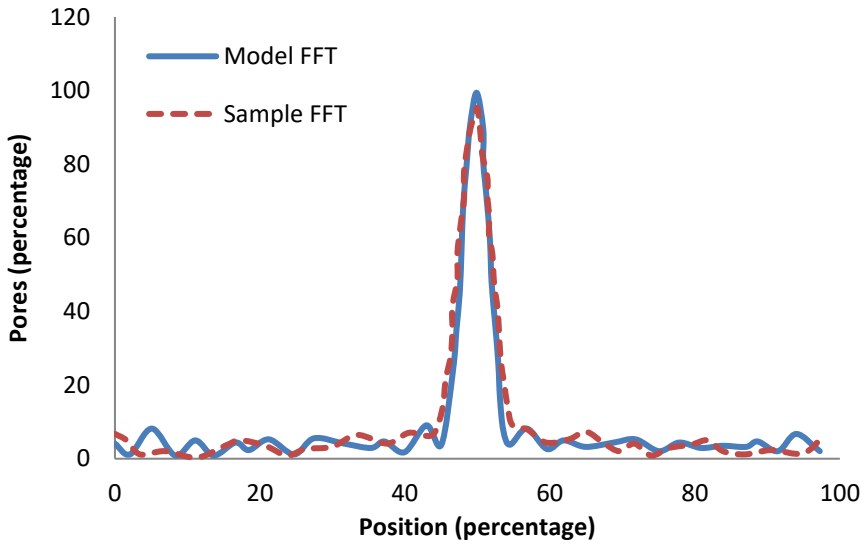

Fig. 2.4. Comparison between FFT of void distribution generated from the actual image and the microstructure created in MATLAB

2.3. Micromechanical Modeling of Pervious Concrete

An APDL code was written to cooperate the microstructure generation and load stress analysis in ANSYS.

2.3.1. Regeneration of Microstructure in Pervious Concrete

Based on the void distribution obtained by FFT, a microstructure of the pervious concrete is regenerated in MATLAB (Fig. 2.5). The void percentage of the regenerated microstructure is kept equal to the void percentage calculated from the actual image. Voids are generated as circles and the number of circles generated in the microstructure is equal to the number of voids in the

actual specimen. As a result, the regenerated microstructure contains the same void percentage and number of voids as the original microstructure (Fig. 2.6). The positions of the voids in the reconstructed microstructure are different from the original one, but they follow the same distribution throughout the entire matrix. The reconstructed microstructure is then imported to ANSYS for load stress analysis through the written APDL code.

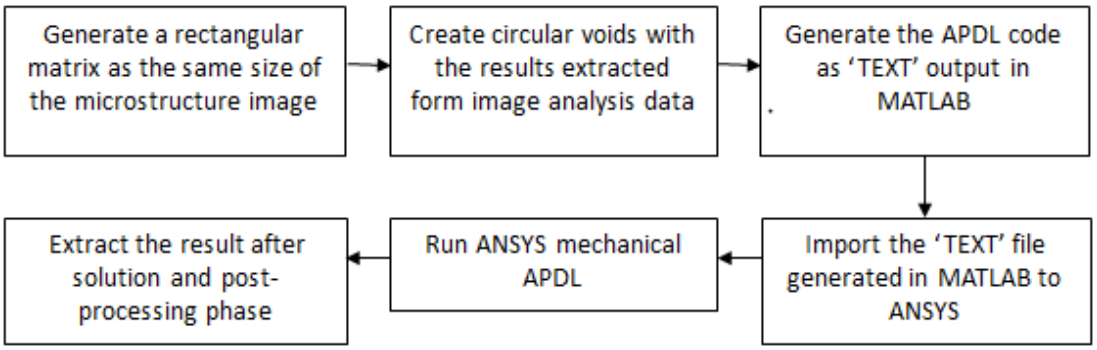

Fig. 2.5. Flow chart of the suggested microstructure regeneration in pervious concrete

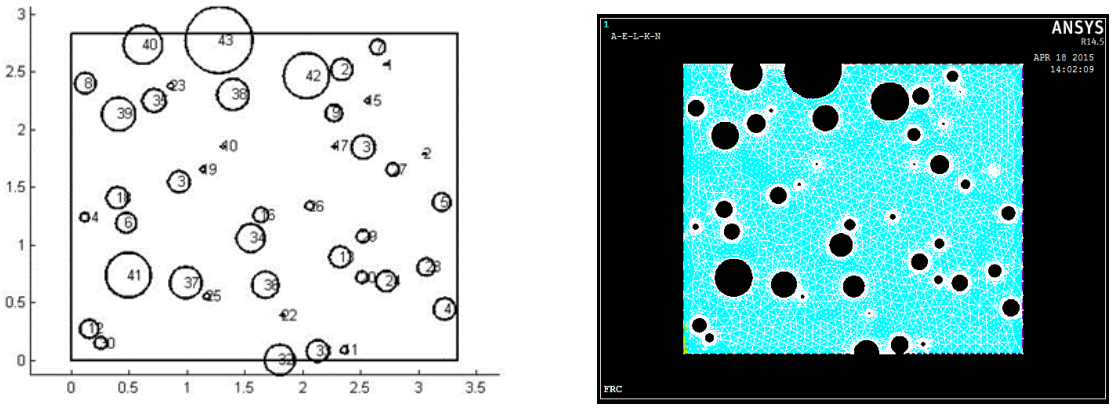

(a) (b)

Fig. 2.6. (a) Void geometry and position in MATLAB using the ImageJ analysis data (matrix size of 3.34 in x 2.83 in, 1 in = 25 mm), (b) porous concrete geometry created in ANSYS

2.3.2. Load Stress Analysis of Pervious Concrete in ANSYS

With the help of mechanical analysis feature of ANSYS, the strength, stiffness and permeability of the concrete specimen were simulated. To model the specimen in ANSYS, element type of PLANE183 is used. This element type is defined by 8 nodes or 6-nodes having two degrees of freedom at each node: translations in the nodal *x* and *y* directions.

The material model of the concrete matrix in the concrete composite is assumed to have a linear elastic and brittle failure behavior. In order to verify the micromechanical modeling technique suggested here, series of lab experiments were conducted to determine the actual concrete parameters and compared with the predicted concrete composite behavior. Thus, most of the concrete parameters used in the model were based on the actual experimental values, with some other conventional parameters determined through literatures. The ANSYS analysis procedure steps are described in the flow chart of Fig. 2.7.

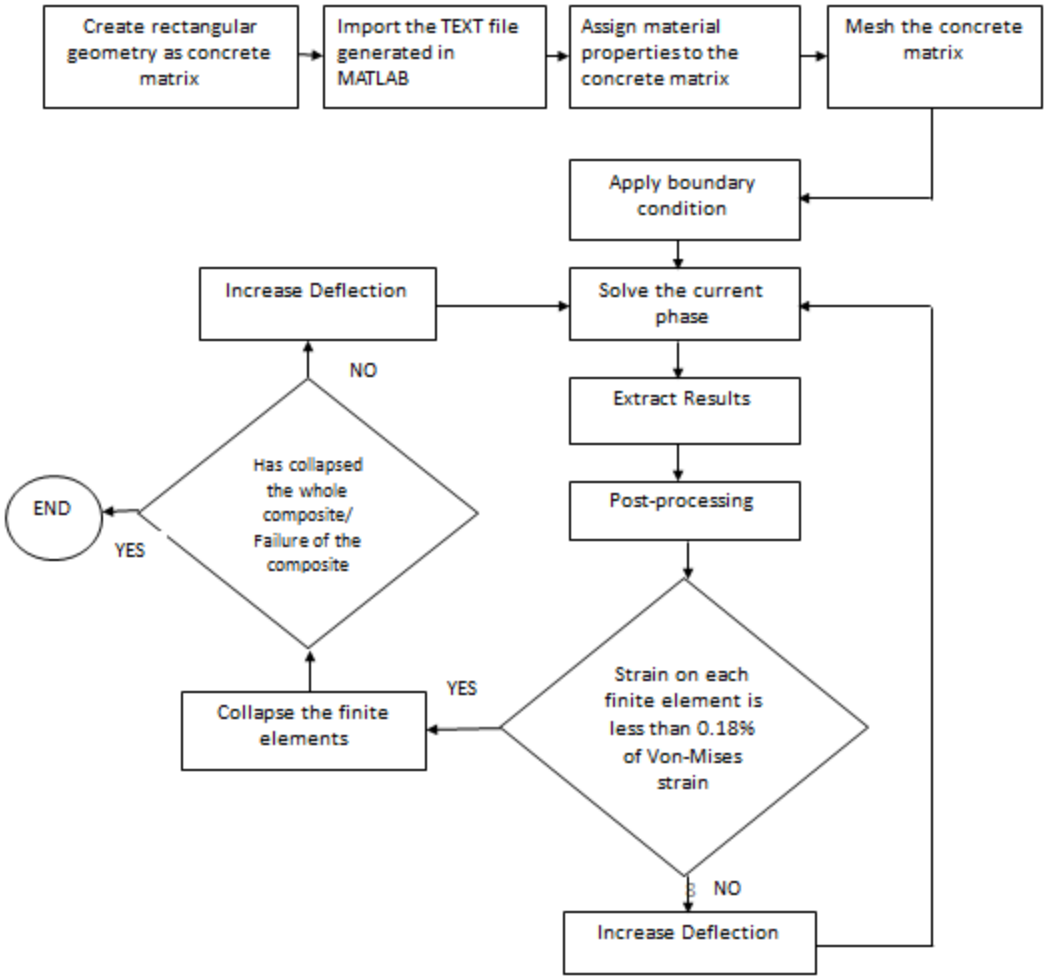

Fig. 2.7. Flow Chart for ANSYS analysis of failure in microstructure modeling of pervious concrete

2.3.3. Permeability Study of Pervious Concrete in ANSYS

Permeability is the measure of distance per unit time that a fluid can pass through a media, which depends on the porosity of the media, viscosity of fluid, and applied pressure gradient. If the fluid velocity is sufficiently low, such as gravity driven flow, Darcy's Law can be adopted to characterize the permeability.

$$K = -\frac{\mu U}{\nabla P} \tag{2.1}$$

where K= permeability of the sample, μ= viscosity of the fluid, ∇P= pressure gradient, U is the fluid flow rate.

The microstructure of porous concrete is generated through MATLAB and then analyzed using the FLOTRAN CFD feature of ANSYS. The boundary conditions were applied in such a way that flow only happened along the pressure gradient direction, but not through the sideways. Uniform pressure was applied at one end (the inlet) and the velocity was measured from the opposite end (the outlet). The pore boundaries were kept as free. The average velocity of the outlet was recorded, and permeability of the specimen is then calculated using Darcy's equation.

2.3.4. Component Material Properties

Pervious concrete composite is a two-phase material with high void percentage and concrete matrix. In order to simulate the concrete matrix accurately, two repeated compression tests were conducted on the pure concrete specimen. The concrete mix ratio used is cement: sand: coarse aggregate of 1:2:4, with a w/c ratio of 0.33.

The experiment is conducted using the 97,860 kN (22.0 kips) Instron tri-axial load frame with a displacement control rate of 2 mm/min. The mechanical properties of the concrete matrix determined through the experiment are shown in Table 2.1 and Fig. 2.8.

Table 2.1. Properties of the concrete matrix

Material	Young's Modulus, *E* (GPa)	Poisson's ratio, *v*	Ultimate strain under compression (material failure) (mm/mm)	Ultimate strain under compression (total failure) (mm/mm)	Ultimate strain under tension (mm/mm)
Concrete	17.0	0.1	0.00075	0.0018	0.00015

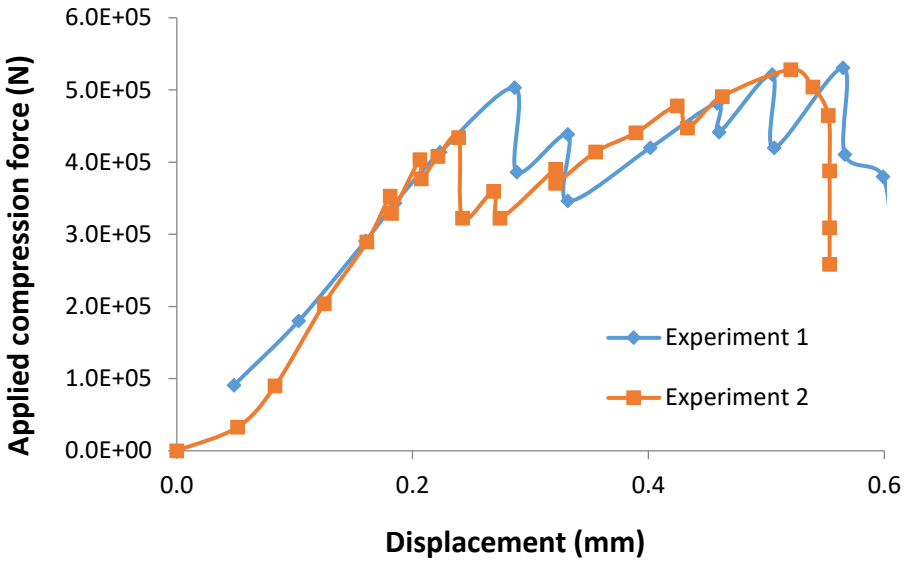

Fig. 2.8. Load-deflection behavior of pure concrete specimen

The ultimate strain of the plane concrete specimen was calculated from the Load-deflection curve generated by the compressive strength testing equipment. The maximum displacement, after which the specimen completely fails to take any further load, was taken and the ultimate strain of 0.0018 mm/mm was obtained. From the load-deflection graph, the material failure strain was taken at the first prominent load drop and calculated as 0.00075 mm/mm, which will be used for further validation purposes.

2.4. Experimental Study

Portland Cement pervious concrete of three different mix ratios (Table 2.2) were tested for obtaining a clear idea on permeability, void ratio, and the 7 days compressive strength of pervious concrete. Three samples for each mix ratio were made and tested accordingly. But only the results from the mix with water/cement ratio of 0.33 are used for comparison.

Table 2.2. Mix ratio used for the Portland cement pervious concrete

Mix	Aggregate Type	Aggregate Size	Cement (kg/m^3)	Aggregate (kg/m^3)	Sand (kg/m^3)	Water (kg/m^3)	Water/cement ratio
1	River Gravel	#4	357	1428	104.8	96.4	0.27
2	River Gravel	#4	371	1484	104.8	111.3	0.3
3	River Gravel	#4	383.5	1534	104.8	126.6	0.33

2.4.1. Materials Used and Specimen Preparation

The pervious cement concrete is made of Portland Cement type I, river gravel (#4 or less than 3/8" (9.5 mm)), and river sand. The cement to coarse aggregate ratio is maintained as 1:4 and a small amount of sand (around 4% of the total volume) is added with the mix.

4"x 8" (ϕ 100 mm x 200 mm) cylinders were used for compression strength tests. 3"x 6" (ϕ 75 mm x 150 mm) cylinders were used to perform the void ratio and permeability tests. Three samples were used for each test. The mixing process is conducted as following: first, a small amount of cement was mixed with aggregate for about 1 minute; second, the remaining cement & water (with or without admixture) was added to the mixture; the mixture was then mixed for three minutes, rested for three minutes, and then mixed for another two minutes before casting. All specimens were placed by rodding 25 times in three layers along with compaction using a standard

compaction hammer for five times after rodding each layer. The samples were de-molded after 24 hours and cured in water.

2.4.2. Experiment Validation Plan

The void content of the concrete samples was determined by taking the difference in weight between a sample oven dry and under water through the following Equation.

$$Vr = \{1- \frac{(W_2 - W_1)}{\rho_w Vol}\} * 100\% \quad (2.2)$$

Where Vr is the total void ratio (%), W_1 is the weight under water, W_2 is the oven dry weight, Vol is the volume of the sample, and ρ_w is the density of water.

Permeability of the concrete samples was determined using the falling head permeability test apparatus. A sample was confined in a membrane and sealed by petroleum gel to ensure no water passes through sideways. Three different water heights were applied to the sample, and the time for the water to drain out of the sample was then recorded. For each water height, the permeability coefficient (K) was determined using Eq. (3). The average value resulting from the different water heights will be defined as the permeability coefficient of the sample.

$$K= (\frac{aL}{At}) \ln \frac{h_1}{h_2} \quad (2.3)$$

where K is the coefficient of permeability, a is the cross sectional area of the water inlet pipe, L is the length of sample, A is the cross-sectional area of specimen, t is the time in seconds from h_1 to h_2, h_1 is the initial water level, and h_2 is the final water level.

Three samples for each mix ratio were tested with the Instron compression strength testing machine and the strength values were directly recorded from the test setup. Based on the supplied specimen size and deformation limit, the Young's modulus, the maximum compressive stress, and the load-deformation curve can be obtained from the test machine (Fig. 2.9).

(a) (b) (c)

Fig. 2.9. Compressive strength testing setup (a) Before loading, (b) Control panel and data acquisition system, (c) after failure

2.5. Results and Discussion

2.5.1. Effect of Gray Threshold on Image Analysis of Microstructure of Pervious Concrete

Void distribution data is extracted through the gray threshold value of the image. It is reasonable to find out that higher porosity was resulted when the gray threshold is increased. Based on the void size and position distribution of images with different gray threshold value, the microstructure of pervious concrete was regenerated through the procedure described above and strength and stiffness for each section was calculated. Both the nominal strength and stiffness of the specimen decrease with the increment of the threshold value (Fig. 2.10 and Fig. 2.11).

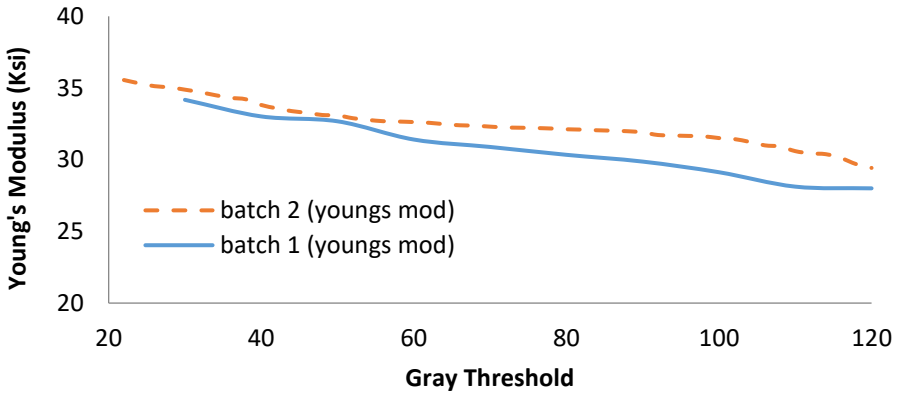

Fig. 2.10. Young's Modulus .vs. Gray Threshold (1.0 ksi = 6.9 MPa)

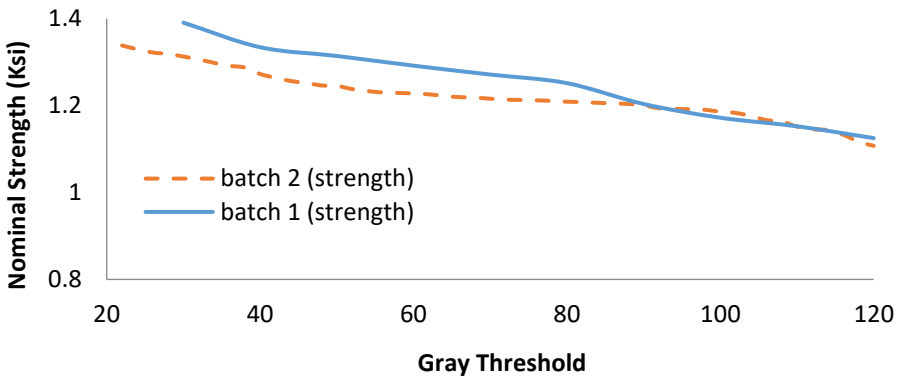

Fig. 2.11. Nominal Strength .vs. Gray Threshold (1.0 ksi = 6.9 MPa)

Lab experiment results of void ratio test show that the void percentage in a pervious concrete specimen ranges from 15~18%, which could be obtained in the regenerated microstructure for gray threshold value ranging from 40~75. Thus, for the rest of the study, the threshold value is taken as 60 (Fig. 2.12).

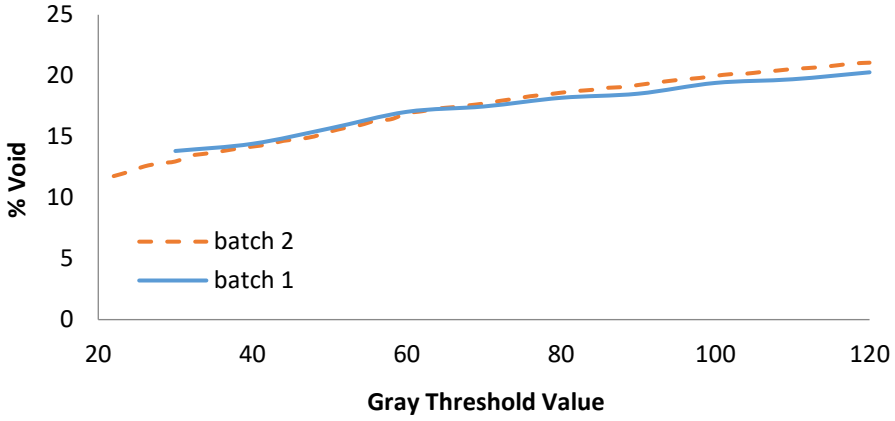

Fig. 2.12. Change in void percentage with increased threshold value.

2.5.2. Correlation between X and Y Coordinate of Void Position

A correlation study is conducted to determine if there is any dependency between the X and Y coordinates of the voids in the microstructure image. The X and Y coordinates of each void is tabulated for different section sizes and the correlation coefficients are calculated to determine the possible dependency between them.

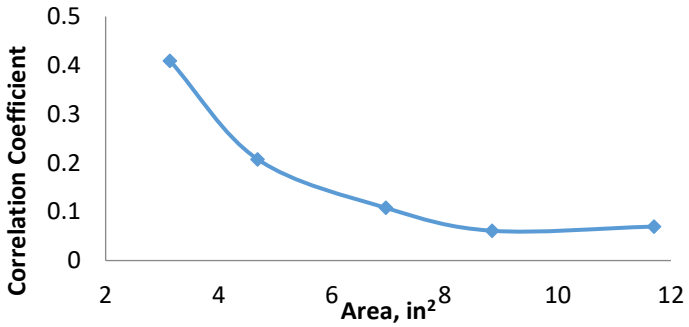

Fig. 2.13. Correlation coefficient .vs. area of the section (1 in^2 = 654 mm^2)

The study shows the correlation coefficients are much below unity, which indicates no dependency between X and Y coordinates of the voids (Fig. 2.13).

2.5.3. Existence of Representative Volume Element

The size of the selected section is gradually increased to obtain a possible representative volume element. As the size of the section is increased, the distribution of voids keeps changing. The sum-square error of relative void positions between two sections shows that void distribution eventually reaches a convergent constant level with increasing of section sizes (Fig. 2.14). At this level, the size of representative volume element is reached.

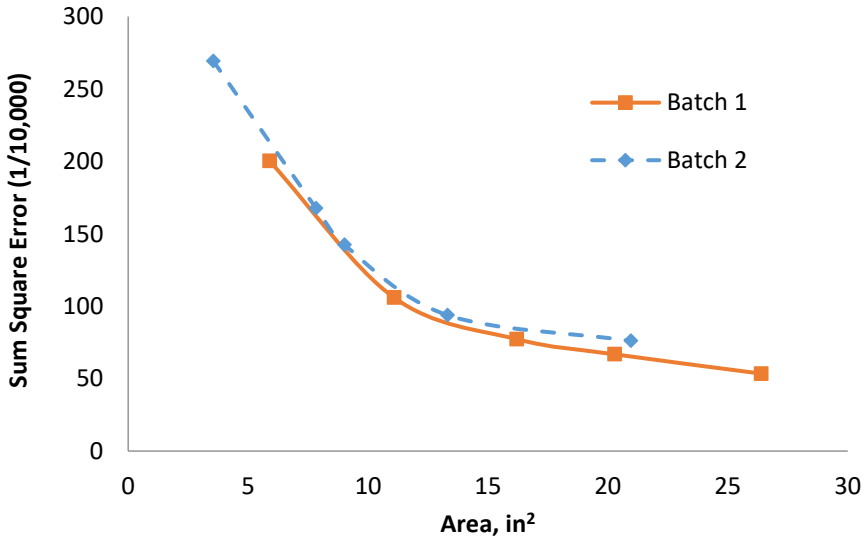

Fig. 2.14. Sum square error of the void distribution .vs. the section area (1 in^2 = 654.2 mm^2)

From Fig. 2.14, for both batch 1 & 2, the square error of void distribution between two sections keep reducing and becomes small enough at a section size around 9677 mm^2 (15 in^2).

2.5.4. Relationship between Compressive Strength and Void Microstructure

A uniaxial compression simulation is conducted for the generated microstructure model with a displacement-controlled boundary condition. The thickness of the section is taken as unity.

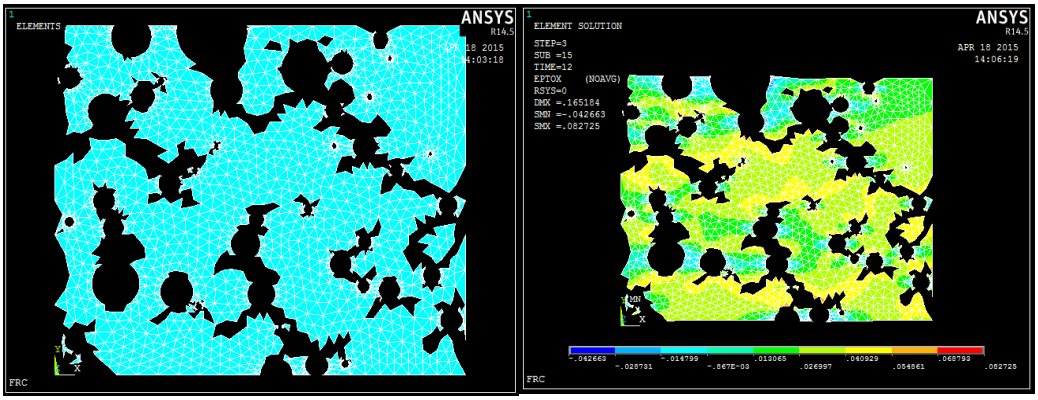

(a) (b)

Fig.2.15. (a) Concrete matrix after failure, (b) Von Mises strain in the concrete matrix

The boundary condition was chosen as a roller support at the bottom surface and fixed at the middle point of that surface. Displacement stroke was applied to the top surface and the other two sides were kept as free. The applied displacement deforms the model, initiates failure and cracks in the concrete matrix (Fig. 2.15). Maximum strain failure criterion is currently selected for this case.

From the model output, the force along the line of applied displacement was obtained and the total force was then used to calculate the strength of the matrix. The change of compression with sizes of sections is shown in Fig. 2.16. As expected, the predicted strength is reduced as the size of section increases. Please note batch 1 and batch 2 have different scanned sizes. The maximum section size could be taken from batch 1 is around 10.0 in^2, which is about half of the scanned size of batch 2.

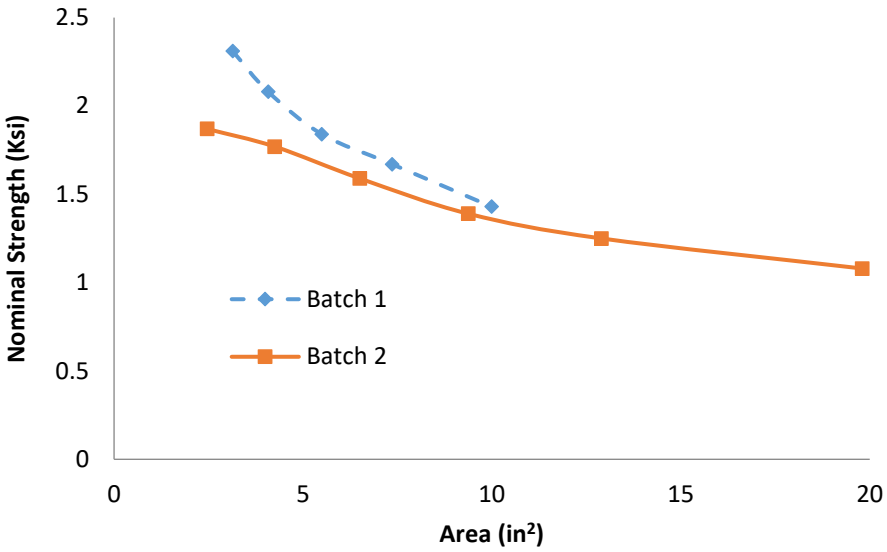

Fig. 2.16. Strength .vs. size of the model section (1 in^2 = 654.2 mm^2, 1.0 ksi = 6.9 MPa)

2.5.5. Relationship between Stiffness of Pervious Concrete and Void Microstructure

The stiffness of the pervious concrete matrix is also calculated. Three simulations for each section are performed and the average value is then reported. Boundary conditions are kept same as discussed in section 5.4. From Fig. 2.17, a decreasing trend is observed and converged at 9677 mm^2 (15.0 in^2) if 0.3% relative difference is defined as the convergence criterion.

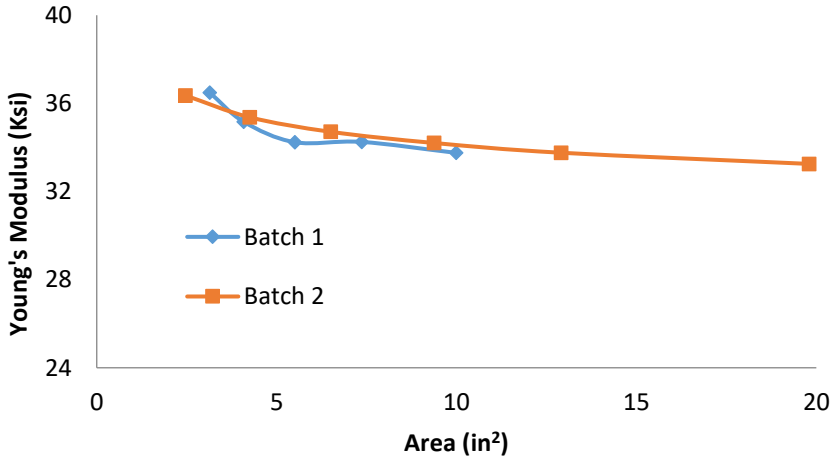

Fig. 2.17. Young's Modulus .vs. section area (1 in^2 = 654.2 mm^2, 1.0 ksi = 6.9 MPa)

2.5.6. Effect of Different Failure Criteria on the Predicted Strength and Stiffness of Pervious Concrete

Failure criteria or modes will affect the prediction of behaviors of pervious concrete. Three different failure criteria, the maximum strain, the maximum stress, and the Von-mises strain failure criteria, are used to evaluate the difference between them.

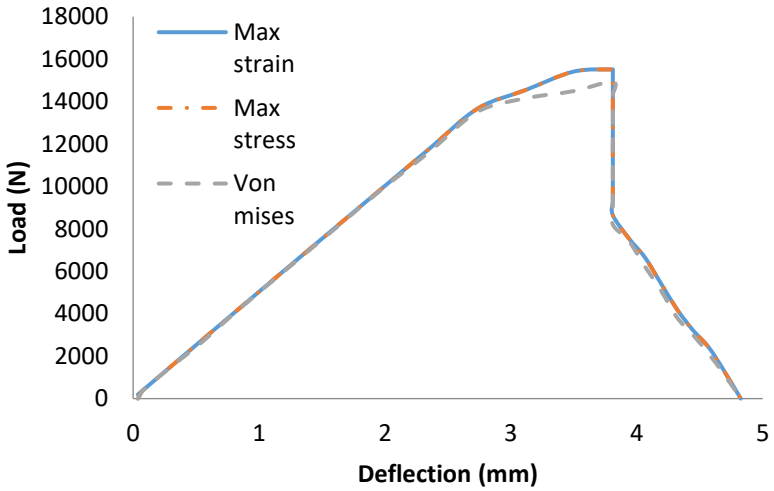

Fig. 2.18. Load-deflection behavior under different failure criterion

The predicted load-deflection plots for the three failure criteria are shown in Fig. 2.18. For the 2D microstructure geometry adopted here, the difference between the maximum strain and Von-mises maximum strain failure criteria is negligible (<5%). For maximum stress and the maximum strain failure criteria, there is no difference since both of them are equivalent uniaxial brittle failure criteria.

2.5.7. Comparison of the Modeling and Experimental Results

In order to prove the suggested micromechanical model as a good approach to predict and optimize pervious concrete, the stress-strain plot predicted through the micromechanical model is compared with the experimental stress-strain plot. The model is based on the maximum strain criterion and the simulation was executed for three different void distributions. The averages of

the three stress-strain values are plotted in Fig. 2.19 and compared with the experiment results from 2 samples of the pervious concrete mix relatively well.

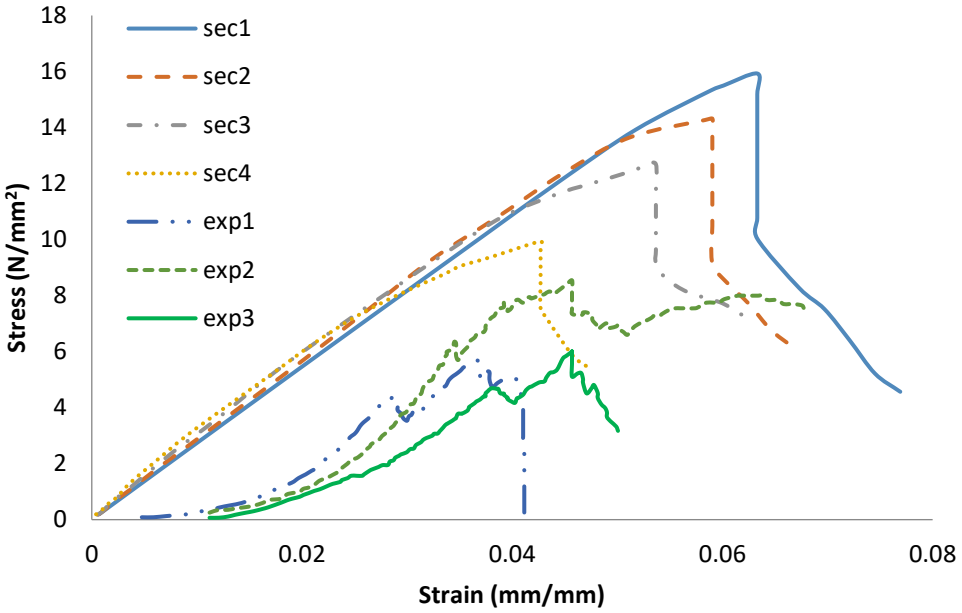

Fig. 2.19. Comparison of stress-strain plot from model and experiments

In Fig. 2.19, sec 1 to 4 stands for the predicted stress strain curve of the different section sizes taken from the mother image from small to big. Exp1, exp2, and exp3 are the stress-strain curves of three physical tests conducted for the pervious concrete mix. A consistent trend of degraded strength with section sizes is observed.

Strength of the specimen under compressive load was defined when the specimen failed to take more load. The comparison between model and experimental results are tabulated in Table 2.3.

Table 2.3. Comparison of the stiffness and compression strength between experiments and modeling (1.0 ksi = 6.9 MPa)

	Young's Modulus	Compression Strength
Experiment	28.88 ksi 29.98 ksi 29.94 ksi	1.047 ksi 1.053 ksi 1.050 ksi
	Mean= 29.60 ksi	Mean= 1.05 ksi
	Standard Deviation= 0.624	Standard Deviation= 0.003
Model	33.07 ksi 32.90 ksi 33.78 ksi	1.19 ksi 1.24 ksi 1.23 ksi
	Mean= 33.25 ksi	Mean= 1.22 ksi
	Standard Deviation= 0.467	Standard Deviation= 0.026

The experimental and model stress-strain plot shows close proximity, even though the stress-strain curves captured by model do not match exactly to that of the experimental failure pattern. In reality, the microstructure has the chance to be condensed and be reorganized when failure starts to occur, which leads to initial small stiffness and regain some strength back when failure starts. In the plot, it shows as the initial concave-up compression consolidation stage and the saw-cut variations of stress after initial failure. However, these phenomena are ignored in the model.

The permeability and porosity relationship from the model is shown in Fig. 2.20. Based on the relationship obtained from the model, the porosity is predicted using the permeability results derived from the laboratory experiments. Fig. 2.21 shows the correlation between predicted and measured porosity.

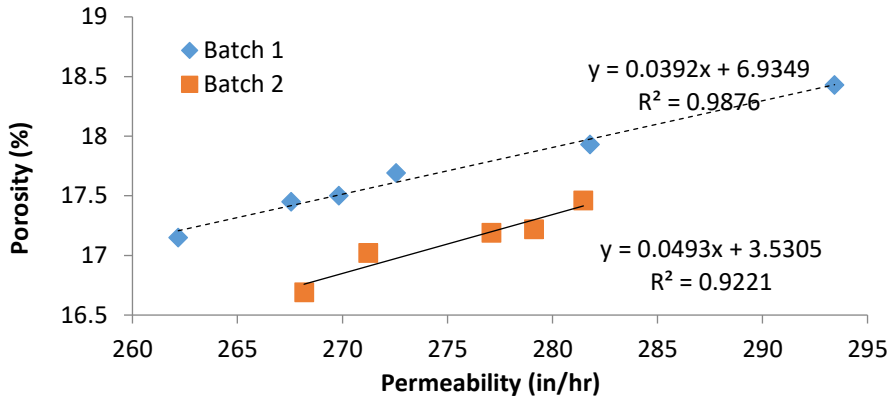

Fig. 2.20. Porosity .vs. permeability predicted from the micromechanical model (1 in = 25.4 mm)

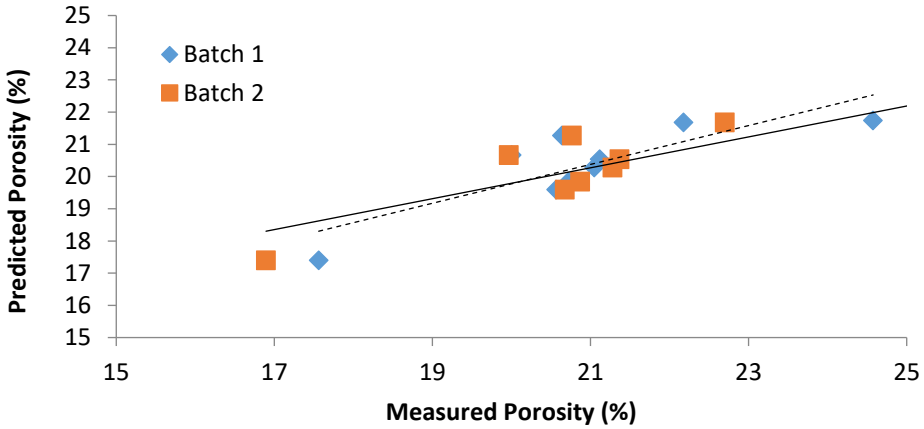

Fig. 2.21. Correlation between the predicted and measured porosity

The predicted porosity from the ANSYS model and the measured porosity through experiments are consistent from Fig. 2.21, which also verifies the suggested micromechanical model.

The model and experimental permeability values are also compared, and the comparison is shown in Table 2.4. The permeability values obtained from experiments and the ANSYS model shows close proximity (error <8%) with each other.

Table 2.4. Comparison of the permeability values between modeling and experiments

		Void Ratio (%)	Permeability from ANSYS model (in/hr)	Permeability from lab experiment (in/hr)	Error (%)
Sample 1	1st repeat	20.28	334.49	360.00	7.08
	2nd repeat	21.30	353.56	349.56	1.14
	3rd repeat	20.54	341.22	361.80	5.69
		Mean= 20.71	Mean= 343.09	Mean= 357.12	Mean= 4.64
		Standard Deviation=0.53	Standard Deviation=9.67	Standard Deviation=6.61	Standard Deviation=3.11
Sample 2	1st repeat	19.60	322.66	347.76	7.23
	2nd repeat	20.67	349.63	333.36	4.88
	3rd repeat	21.68	360.66	388.80	7.24
		Mean= 20.65	Mean=344.32	Mean= 356.64	Mean= 6.45
		Standard Deviation=1.04	Standard Deviation=19.55	Standard Deviation=28.77	Standard Deviation= 1.36

In summary, the image based micromechanical modeling could be used to predict pervious concrete properties after careful calibration of the gray threshold and representative section size. The derived stiffness, strength, and permeability are highly close to the physical testing values.

2.6. Conclusions

In this paper, a study focusing on imaged based micromechanical analysis of pervious concrete composite is performed. The effect of gray threshold in image analysis of void ratio is first discussed and compared with physical experiments. Void size distribution and void position distribution are then analyzed through FFT and regenerated through a MATLAB code. Existence of representative volume element is also found to be around 9677 mm^2 (15 in^2). The macro mechanical properties such as compression strength, stiffness, and permeability of the regenerated pervious concrete matrix are then predicted and summarized with change of sizes. It was found that the predicted stiffness, strength, and permeability of pervious concrete are in close match with physical experimental results.

2.7. References

[1] Chopra M., Wanielista M. and Mulligan A. M., (2007a). Performance assessment of Portland cement pervious pavement, Final Report, FDOT Project BD521-02.

[2] Chopra M., Wanielista M. and Mulligan A. M., (2007b). Compressive Strength of Pervious Concrete Pavements , Final Report. A Joint Research Program of FDOT, Rinker Materials and FDEP.

[3] Chopra M., Wanielista M., (2007c). Performance Assessment of a Pervious Concrete Pavement Used as a Shoulder for a Interstate Rest Area Parking Lot, Final Report. A Joint Research Program of FDOT, Rinker Materials and FDEP.

[4] Yang J., and Jiang G., (2003). Experimental Study on Properties of Pervious Concrete Pavement Materials, Cement and Concrete Research, 33: 381–386.

[5] Kevern J. T., Wang K., and Schaefer V. R., (2010). The Effect of Coarse Aggregate on the Freeze-Thaw Durability of Pervious Concrete, ASCE Journal of Materials in Civil Engineering, 22 (5): 469-475.

[6]] Kevern J. T., Schaefer V. R., Wang K., and Suleiman M. T., (2008). Pervious Concrete Mixture Proportions for Improved Freeze-Thaw Durability, Journal of ASTM International, 5(2): Paper ID JAI101320.

[7] Made A.M., and Rogge S., (2013). Development of High Quality Pervious Concrete Specifications for Maryland Conditions, Final Report, Project Number SP009B4F.

[8] Hu J., and Stroeven P., (2003). Application of Image Analysis to Assessing Critical Pore Size for Permeability Prediction of Cement Paste, Image Anal Stereol, 22:97-103.

[9] Wong H.S., Head M.K., Buenfeld N.R., (2006). Pore segmentation of cement-based materials from backscattered electron images, Cement & Concrete Research, 36 (6): 1083-1090

[10] Lange D. A., Jennings H. M., Shah S. P., (1994). Image Analysis Techniques for Characterization of Pore Structure of Cement-Based Materials, Cement and Concrete Research, 24(5):841-853.

[11] Igarashi S., Chen W., Brouwers H.J.H. (2009). Comparison of observed and simulated cement microstructure using spatial correlation functions, Cement & Concrete Composites, 31: 637–646.

[12] Collins T. J., (2007). ImageJ for microscopy, BioTechniques. 43: 25–30.

[13] Moulinec H., Suquet P., (1994). A fast numerical method for computing the linear and the nonlinear mechanical properties of composites, Com. Res. Acad. Sci. Paris II, 38(11): 1417–1423.

[14] Bilger N., Auslender F., Bornert M., Michel Jean-Claude, Moulinec H., Suquet P., Zaoui A., (2005). Effect of a nonuniform distribution of voids on the plastic response of voided materials: a computational and statistical analysis, International Journal of Solids and Structures, 42:517–538.

CHAPTER 3. EFFECTIVENESS OF CHEMICAL TREATMENT ON CHAPTER POLYPROPYLENE FIBERS AS REINFORCEMENT IN PERVIOUS CONCRETE

3.1. Introduction

Fiber reinforcement delays the crack generation and enhances the strength of the host matrix. However, the bonding mechanism between fiber and concrete matrix is controversial in literature and needs better explanation. Due to surface smoothness and inert chemical nature of commercially available fibers, several mechanical and chemical treatment techniques have been studied by researchers to increase the fiber-matrix bonding properties. The use of fibers in pervious concrete is even more challenging due to high porosity and insufficient fiber-matrix bonding interface. This study discusses the effect of chemical treatment on short polypropylene fibers and its uses in pervious concrete as reinforcement. The change in fiber surface due to the treatment is determined through fiber wettability test and Atomic Force Microscopy (AFM). Changes on the tensile strength of fibers by the treatment methods are also tabulated. Single fiber pullout tests are conducted to study the effect of the treatment type on fiber-cement interface properties. Treated fibers are then put into pervious concrete matrix for compressive and flexural strength tests. Chemical treatments are found to improve the surface roughness and cement matrix interface properties, as well as to enhance the overall strength of the fiber reinforced pervious concrete.

Polypropylene fibers are widely used as reinforcement in concrete composites due to their superior properties over other fibers. Commercially available polypropylene fibers offer high melting point and better chemical stability than other fiber types such as steel or fiberglass fibers, and the cost is relatively less. These fibers are used as secondary concrete reinforcement to restrict the initiation and propagation of shrinkage cracks. However, being hydrophobic in nature, polypropylene fibers often result in poor bonding with the concrete composites.

By adding the polypropylene (PP) fibers to concrete, it is possible to improve the tensile strength of the concrete. Reinforcing PP fibers can improve the durability of the concrete matrix by increasing the ductility and absorbing energy when subjected to impact loads and external vibrations (Fischera et al., 2007). However, polypropylene chain structure is chemically inert, hydrophobic and has low surface energy. These characteristics of polypropylene are caused by the presence of non-polar methyl group CH_3, bonded to the chain of carbon atoms. After mixing the PP fibers into the concrete mixture, the fibers will form clusters and the equal distribution cannot be achieved. Clusters of fibers often trap considerable amount of air, which has an adverse effect on the mechanical properties of the fiber-reinforced concrete (Peled, et al., 1992). Therefore, researchers have adopted several chemical treatment processes to increase its surface energy. Plasma treatment is one of the eco-friendly approaches to increase the surface energy of polypropylene fibers.

Zheng et al., (1995) studied the use of relatively low-modulus polypropylene fibers (without any mechanical/chemical) treatment in concrete matrix. The results showed that there were no considerable improvements in the tensile strength. However, the flexural strength, toughness, and ductility in concrete were significantly improved. Concrete reinforced with collated and fibrillated polypropylene fibers at a relatively low volume fraction are usually used as secondary temperature shrinkage reinforcement, crash barriers, slabs, overlays, and pavements. The fiber-concrete initial bonding can be affected by both the mechanical bonding properties of fiber and the static friction inherited by the fiber surface (Martinez-Barrera et al., 2005). Chemical bonding between the fibers and the matrix are found to be weaker in comparison with the fiber's resistance to friction against the pull-out (Kopczynska et al., 2007). Also, most fiber deformation and degradation processes initiate local mechanical interactions between fiber and matrix, which

leads to a redistribution of the load by the matrix. Fibers tend to arrest crack generation through the initial loading stages and keeps increasing the required energy for crack propagation. Thus, it provides an increment in the flexural strength. During the later stages of straining, the fibers redistribute the microcracking, thus increasing toughness and ductility.

The main disadvantage of using polypropylene fibers as a reinforcement is their non-polar nature (Carstens et al., 2000), which prevents adhesion to concrete matrix. Several methodologies in literature have used shrinkage reducing admixtures, which help to increase compatibility of polypropylene fibers and limit crack width (Mora-Ruacho et al., 2009). The key factor to obtain good mechanical properties for fiber reinforced concrete is the interfacial adhesion between the concrete matrix and the fiber (Mohanty et al., 2002, Zafeiropoulos, et al., 2002). Mechanical modifications, such as fibrillations and fiber indentation increase the bonding with cement matrix. Surface treatments can modify the fiber/concrete interface by roughening the fiber surface and altering surface polarity (Zhang et al., 2000). The modification of the surface chemistry and morphology through chemical treatment can increase the interfacial bond strength in comparison with the untreated PP fiber-concrete matrices.

Regarding techniques used in testing fiber reinforced concretes (FRC), many reports cite the improved static strength characteristics of such composite systems (Sheldon, 1982). However, results of compression testing of fiber reinforced concrete reported by some researchers have shown conflicting information. Early reports, such as those by Hannat et al. (1978), found that concrete without fiber reinforcement is stronger in compression compared to polypropylene fiber reinforced concrete. It was later reported by Fialova, et al. (2012) that polypropylene fiber reinforced concrete (PFRC) reaches to a higher compressive strength after 28 days of cure time than that of plain concrete. Several researchers (Aly et al., 2008) in the FRC field explained that

standard uniaxial compression testing should not be the only test method used to conclude on the mechanical properties of such composites. Other mechanical test methods, such as flexural strength tests should be conducted to determine the static strength characteristics of FRC composites.

In this work, the short polypropylene fibers were chemically treated to enhance the fiber-matrix interface properties and used in pervious concrete to study its effect on the compressive and flexural strength. First, the effect of chemical treatments on the PP fiber is discussed. Then fiber pullout tests were conducted on both treated and untreated fibers to study the change in fiber-cement matrix interface properties. Chemically treated fibers were then analyzed with Atomic Force Microscopy (AFM) for evaluating the enhancement of surface roughness. Both compressive and flexural strength tests were then carried out with cylinder and beam specimens, respectively, and results were reported.

3.2. Materials and Methods

3.2.1. Properties of Polypropylene Fiber

ProCon-F-E polypropylene fibers, manufactured by Nycon have been used throughout the study. ProCon-F-E is a cost-effective fiber that provides plastic shrinkage and settlement crack control, increased impact resistance and residual strength. The physical properties of the polypropylene fiber are listed in Table 3.1.

Table 3.1. Physical properties of polypropylene fibers used

Filament Diameter	0.03” (0.76 mm)
Fiber length	0.75” (19.00 mm)
Specific Gravity	0.91
Tensile Strength	44 ksi (300 MPa)
Flexural Strength	700 ksi (4.90 GPa)
Melting Point	320^{o} F (160^{o} C)
Color	White
Alkali Resistance	Excellent
Corrosion Resistance	High

3.2.2. Chemical Treatment of Polypropylene Fibers

Polypropylene fibers are used for cement reinforcement in two ways (Peled et al., 2005): (a) As a primary reinforcement, with 5-10% fiber content by volume. Polypropylene fibers are used as a mesh or fabric in such applications, which yields continuous reinforcement. (b) As a secondary reinforcement, with short fibers and lower content by volume (less than 0.3%).

Polypropylene fibers have a hydrophobic surface and its modulus of elasticity is lower than that of cement matrix. As a matter of fact, it is assumed that there is no existence of physio-chemical adhesion bonding between polypropylene fibers and cement when they are mixed

together. In this study, four different treatments are evaluated in terms of their effect on the mechanical properties of fiber reinforced pervious concrete.

1. Porofication treatment -- the monofilament fibers were dipped in a Br_2+H_20 (10-11 ml/liter) solution for 24 h at 20^oC and then placed in an ammonia solution for 1 h at 40°C. The fibers were washed with water and dried at room temperature. This treatment may induce a rough and porous surface (hence it is called 'porofication') and increase the fiber surface area.
2. Treatment with surface-active agents (detergent) -- the monofilament fibers were dipped in a solution of nonionic detergent (Triton X-100, 0.1% concentration) in water for 10 s, and dried at room temperature. This treatment was applied to enhance the wetting properties of the polypropylene fiber's surface and intended to improve the fiber compatibility with the matrix.
3. Treatment with polyvinyl acetate (PVAC) -- after the porofication treatment the monofilament fibers were dipped in a 5% PVAC solution in water for 10 s and dried at room temperature. This treatment was provided to achieve better adhesion between the polypropylene fibers and the cement matrix through a PVAC layer. The porofication treatment was carried out so that the PVAC coat on the fiber's surface would be homogeneous.
4. Sulphuric acid-dichromate treatment -- the monofilament fibers were dipped into a bath of 10% sulphuric acid and sodium dichromate solution for 18 h at 50°C and then washed with water and dried at room temperature. This treatment might cause asperity on the fiber surface and may introduce a chemical reaction and bonding between the polypropylene fibers and the cement matrix.

3.2.3. Wettability of Polypropylene Fiber

Wettability of a solid surface is the capability of liquid to adhere to the surface and it is related to the molecular interaction characteristics of both solid and liquid phases. Researchers have adopted two processes to measure the wettability of polypropylene fibers, contact angle determination and water absorption (Darmanin et al. 2014). Orchon et al. (1958) introduced the contact angle determination methodology for the first time. It was then used to explain surface tension, wettability, glueability, paintability, and laminating properties of the materials (Lundquist et al., 2003, Diehl et al., 2005). Mohebby et al. (2011) adopted the water absorption technique to measure the polypropylene fiber wettability. In Mohebby's study, both treated and untreated fibers were dried at 103±2°C to determine dry weights prior to water soaking test. The fibers were then soaked in distilled water at room temperature (25°C) and weighed at a time interval 2, 4, 6, 12 and 24 hours to determine their wet weights (wet fibers were placed on a wire bucket so the excess water can flow through, but the water trapped on the fiber surface remains). Water absorption is calculated according to Eq. 3.1:

$$A\ (\%) = \frac{W_w - W_0}{W_0} * 100\% \tag{3.1}$$

where A is water absorption (%), W_w and W_o indicate wet weight and dry weight of the specimens (g), respectively.

In this study, the same method is adopted to determine the wettability of treated and untreated polypropylene fibers.

3.2.4. Single Fiber Pullout Test

Fiber reinforcement can be very efficient for improving tensile response of concrete composite, through bridging mechanisms over cracks of different widths. Single fiber pullout test is one of the most commonly used techniques to characterize the fiber-cement matrix interface properties. In this study, single fiber pullout tests have been carried out for treated and untreated polypropylene fibers. The fiber used in this test is 19 mm in length with a diameter of 0.76 mm. The fiber embedded length was controlled at 12 mm.

To derive the fiber-matrix interface properties, Eq. 3.2 is used:

$$\tau = \frac{P_{max}}{2\,\pi r\, l_e} \tag{3.2}$$

where, τ is the average interfacial shear strength, P_{max} is the maximum force from the force-displacement plot, r is the fiber radius, and l_e is the fiber embedded length.

Shear-lag theory has been used to derive the bond strength and frictional strength of fiber-matrix interface (Laws, 1982). First, the slope, S, of the initial linear part of the force - displacement plot is calculated. Then, the parameter β_1 is solved numerically according to Eq. 3.3:

$$S = \frac{\beta_1 . E_f . A_f . sinh\left(\frac{\beta_1 . l_f}{2}\right)}{cosh\left(\frac{\beta_1 . l_f}{2}\right) - 1} \tag{3.3}$$

Where, E_f is the elastic modulus of fiber, A_f is the fiber area, and l_f is the fiber embedded length. The bond strength, τ_s, is calculated using Eq. 3.4:

$$\tau_s = \frac{\beta_1 . P_A}{\pi . d_f . tanh(\beta_1 . l_f)} \tag{3.4}$$

Where, d_f is the fiber diameter and P_A is the elastic limit from the force-displacement plot. The maximum pullout load, P_B, from the force-displacement plot can be expressed by Eq. 3.5:

$$P_B = \pi . d_f \left[\frac{1}{\beta_1} \sqrt{\tau_s^2 - \tau_f} + \tau_f \frac{l_f}{2} - \tau_f . atanh \left(\sqrt{1 - \frac{\tau_f}{\tau_s}} \right) \right] \quad (3.5)$$

Then the equation is finally solved numerically for frictional bond strength, τ_f.

3.2.5. Specimen Size Design for Single Fiber Pullout Test

The fixed boundary provided through the left vertical face will affect the stress distribution along the fiber matrix interface when conducting the fiber pullout test. In order to minimize the effect of boundary on the experimental fiber pullout test results, different fiber end to the boundary distances (x) of the single fiber pullout test was simulated through a 2-D ANSYS model (Fig. 3.1).

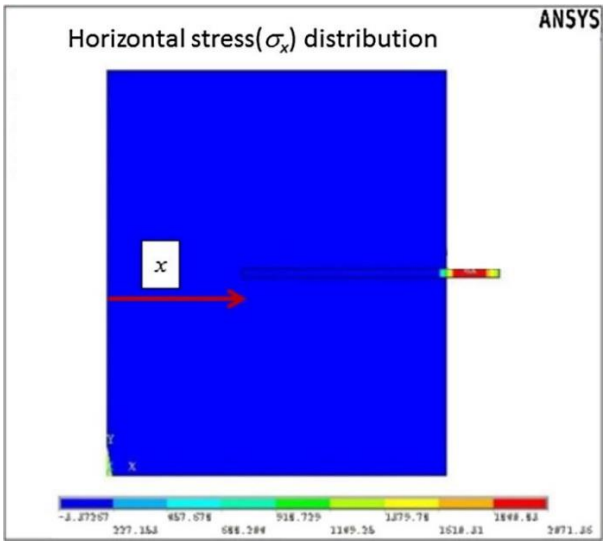

Fig. 3.1. ANSYS model to simulate single fiber pullout test.

By varying the distance between the fiber end and the left vertical face of the specimen, the stress at the left vertical face of the specimen varies. If the stress along the left vertical surface is uniformly constant, it means a uniform far field stress has been reached and no effect would be expected on the interface stress distribution between the fiber and the matrix.

In ANSYS, element type of PLANE183 is used to model the specimen. This element type is defined by 8 nodes or 6- nodes having two degrees of freedom at each node: translations in the nodal x and y directions.

When applied with a horizontal equivalent stress of 2 psi (2 lb force on the fiber for a 1x1x1'' (25.4x25.4x25.4 mm) specimen), the horizontal stress distribution along the left vertical surface is shown in Figure 24. If 5.0% difference with the uniform far end stress state is used as the threshold, the plot shows a 0.4 in (11.6 mm) distance between the fiber end and the left vertical face of the specimen is sufficient to minimize the effect of left vertical face on the pullout testing results (Fig. 3.2). In this study, a 1x1x1'' (25.4x25.4x25.4 mm) specimen and 0.5'' (12.7 mm) distance between the fiber end and the left vertical face of the specimen are selected.

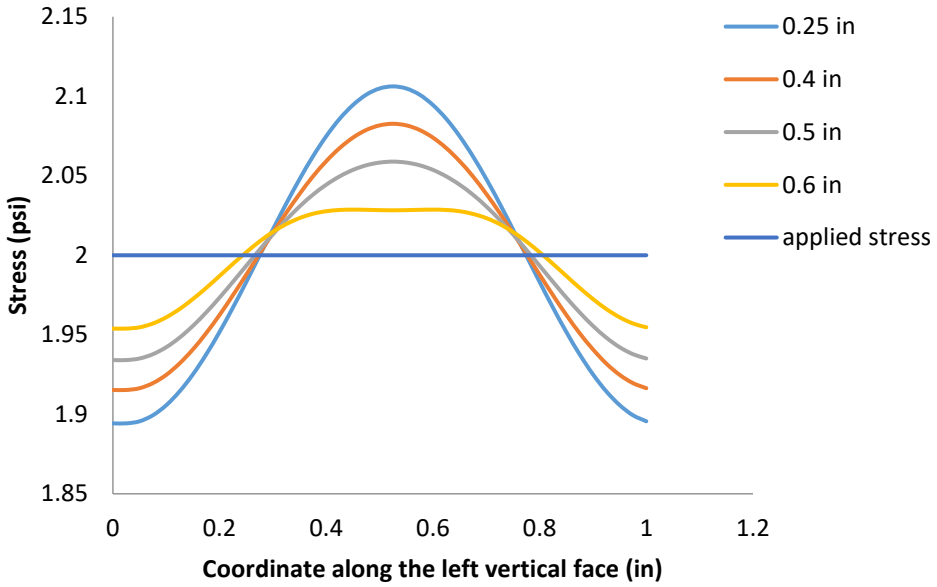

Fig. 3.2. Stress distribution at the left vertical face of the cement matrix specimen due to different distance between the fiber end and the left vertical face (1psi = 0.0069 MPa, 1 inch = 25.4 mm)

3.2.6. Compression Strength Test

The pervious concrete is made of Portland Cement type I, river gravel (#4 or less than 9.525 mm), and river sand. The cement to coarse aggregate ratio is maintained as 1:4 and a small amount of sand (around 4% of the total volume) is added to the mixture. The mix composition of different pervious concrete adopted in this paper is shown in Table 3.2.

4.0 x 8.0 in. cylinder (Φ101.6 x 203.2 mm) samples were used for compression strength tests. Three samples were used for each test. The mixing process is conducted as following (Kevern et al., 2005): first, a small amount of cement was mixed with aggregate for about 1 minute; second, the remaining cement and water, with polypropylene fibers dispersed in it (with or without admixture), was added to the mixture. The materials were then mixed for three minutes, rested for three minutes, and then mixed for another two minutes before casting. All specimens were placed by rodding 25 times in each of the three layers along with compaction using 5.5 lb standard compaction hammer for five times after rodding each layer. The samples were de-molded after 24 hours and cured under water for 7 days, following with curing at 50% humidity, 20^{o}C for 21 days. The experiment is conducted using the 97,860 kN (22.0 kips) Instron tri-axial load frame with a displacement control rate of 2 mm/min.

Table 3.2. Mix ratio used for Portland cement pervious concrete

Mix	Aggregate type	Aggregate size	Cement (kg/m^3)	Aggregate (kg/m^3)	Sand (kg/m^3)	Water (kg/m^3)	Water/cement ratio	Fiber Volume
1	River gravel	#4	357	1428	104.8	96.4	0.27	1%
2	River gravel	#4	371	1484	104.8	111.3	0.30	1%
3	River gravel	#4	383.5	1534	104.8	126.6	0.33	1%

3.2.7. Void Ratio Test

The void content of the concrete samples was determined by taking the difference in weight between a sample oven dry and under water through the following Equation.

$$V_r = \left\{1 - \frac{(W_2 - W_1)}{\rho_W * Vol}\right\} * 100\% \quad (3.6)$$

Where, V_r is the total void ratio (%), W_1 is the weight under water, W_2 is the oven dry weight, *Vol* is the volume of the sample, and ρ_W is the density of water.

3.2.8. Flexural Strength Test

Flexural strength tests of polypropylene fiber reinforced pervious concrete beam specimen were carried out following the guidelines of ASTM C78/C78M (2016), which uses a simple beam with third point loading. Pervious concrete beams of size 150 x 150 x 500 mm were casted with addition of 2% polypropylene fiber by volume. Two beams were casted for each fiber treatment cases. Beams were casted in two layers with 50 times rodding in each layer. De-molded beams were cured under water for 7 days and then tested for flexural strength (beams were taken out of water 2-3 hours prior to the test and the excess water was allowed to drain). Modulus of rupture was calculated for each beam and the results were compared for chemically treated and untreated fiber reinforced cases.

As the fracture was initiated in the tension surface within the middle third of the span length, the modulus of rupture is calculated according to Eq. 3.7:

$$R = \frac{PL}{bd^2} \quad (3.7)$$

Where R = modulus of rupture, psi (MPa); P = maximum applied load indicated by the testing machine, lbf (N); L = span length, in. (mm); b = average width of specimen, in. (mm), at the fracture, and d = average depth of specimen, in. (mm), at the fracture.

3.3. Results

3.3.1. Fiber Wettability Test

For porofication treatment, fibers were dipped in bromine (Br_2 +H_2O) solution with varied concentration of 5 ml/L, 10 ml/L and 15 ml/L respectively. The water absorption was then measured over the described time interval.

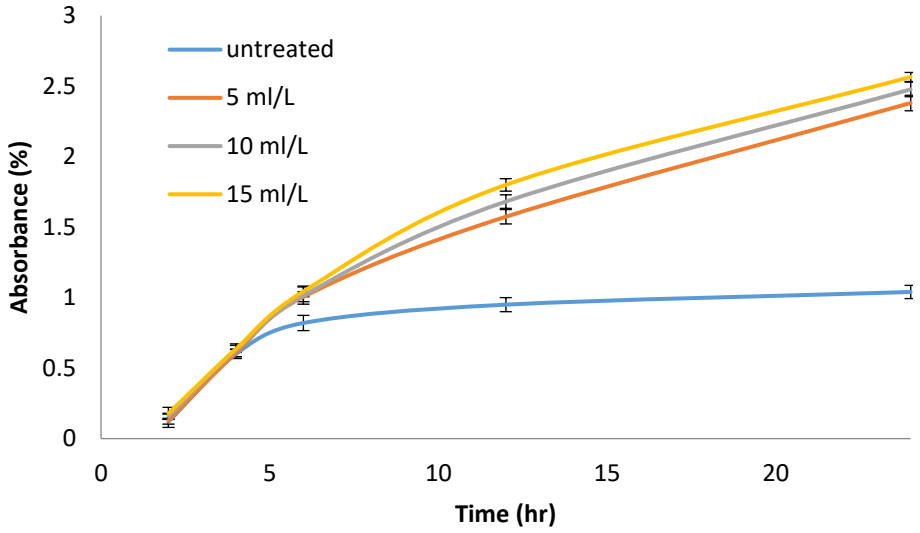

Fig. 3.3. Change in water absorption (%) over time due to Porofication treatment.

The change in absorption of water on the fiber surface due to the varied concentration of bromine solution is between 4~8% with respect to that of untreated fibers, as shown in Fig. 3.3. With higher concentration of bromine solution, the absorbance was found having higher absorbance value. After 24 hours, the (%) absorbance was in between 2 to 2.5% for bromine concentrations of 5 ml/L to 15 ml/L, whereas, untreated fibers have absorbance of 1.04% after 24 hours.

For treatment with surface-active agents (detergent), fibers were dipped into the detergent solution of three different concentration of 0.1%, 0.2% and 0.3% respectively. The soaking time was also varied for 5s, 10s and 15s.

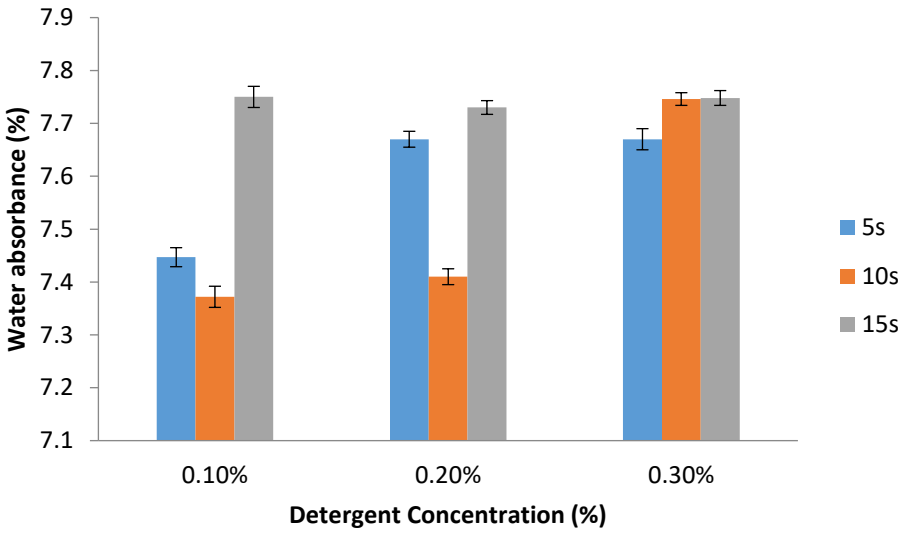

Fig. 3.4. Change in water absorbance after 24 hours in detergent treated polypropylene fibers.

The water absorbance of the fiber ranges from 7.1~7.8% after 24 hours, whereas the untreated fibers have a water absorbance of 1.04%, as shown in Fig. 3.4. Also, from Fig. 3.4, it is possible to see that the absorbance percentage is almost the same for varying detergent concentrations at a soaking time of 15s. The increased water absorbance indicates the change in surface energy of the fibers due to the treatment process.

For treatment with Polyvinyl Acetate (PVAC), the concentration of PVAC solution was varied as 3%, 10% and 20% with a variable soaking time of 10 s, 20 s and 30 s.

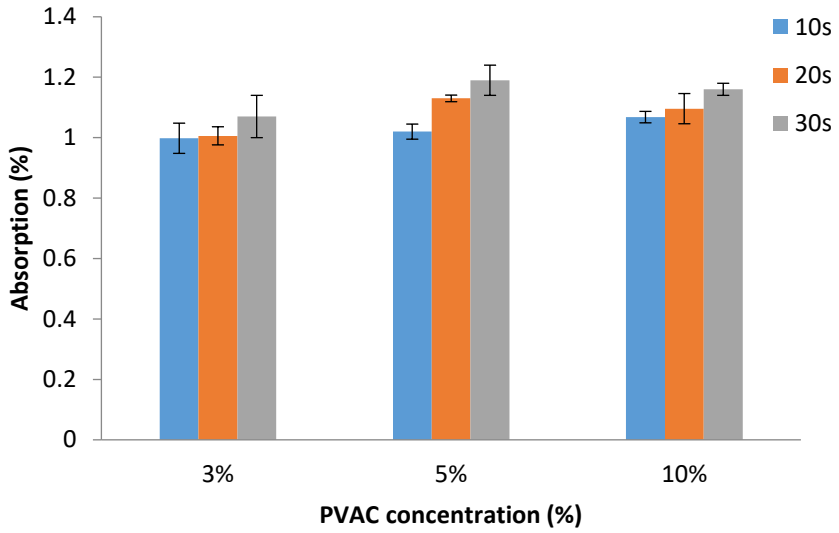

Fig. 3.5. Change in water absorbance after 24 hours in PVAC treated polypropylene fibers.

PVAC creates a coat on the polypropylene fiber surface. As a result, the water absorption after PVAC treatment is not significantly improved than the absorption of untreated fibers (~1.04% absorbance), as shown in Fig. 3.5.

For Sulfuric acid-dichromate treatment, fibers were treated with the Sulphuric acid-Sodium dichromate solution of concentrations varied as 10%, 20%, and 30%. Three different soaking times (8 hours, 16 hours and 24 hours) have been used to study the effect of different soaking times.

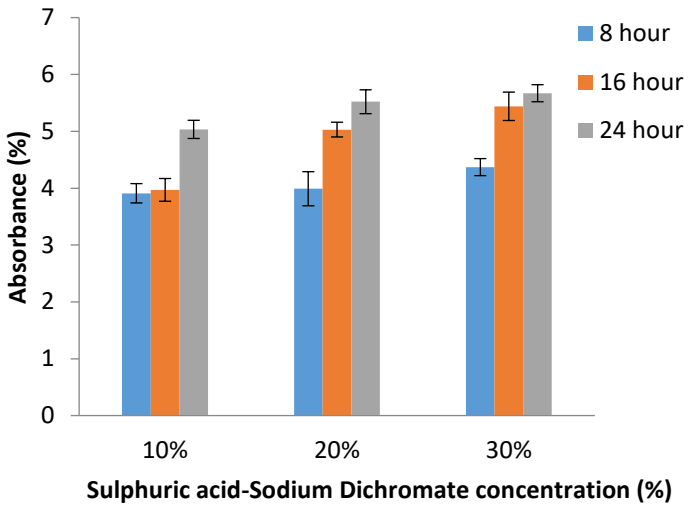

Fig. 3.6. Change in water absorbance after 24 hours in acid treated polypropylene fibers

The acid treatment causes porosity and harshness to the fiber surface which eventually increases the wettability of the fiber. As shown in Fig. 3.6, the absorbance of acid treated fibers ranges from 3~6%, which is much higher than that of untreated fibers (absorbance ~1.04%).

The comparisons of untreated fibers with fibers treated with different chemical methods are tabulated in Fig. 3.7. The water absorbance is significantly improved by bromine, detergent and acid treatment but the PVAC treatment fails to enhance the wettability due to a coating of PVAC on the fiber surface.

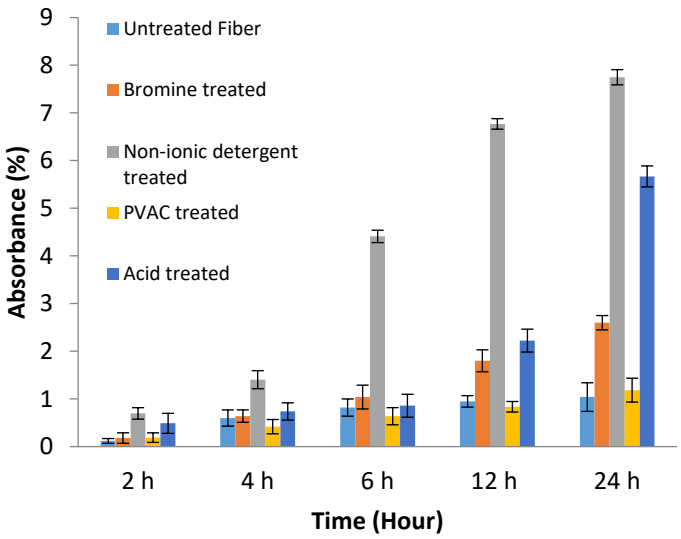

Fig. 3.7. Comparison of water absorbance (%) due to different fiber treatment processes with untreated fibers.

3.3.2. Fiber Pullout Test

Force-displacement plots were generated through the single fiber pullout test of untreated and chemically treated fibers. The plots were then used to derive fiber-matrix interface properties such as average interfacial shear strength (τ), bond strength (τ_s), and frictional bond strength (τ_f). The typical force-displacement response due to single fiber pullout tests is shown in Fig. 3.8.

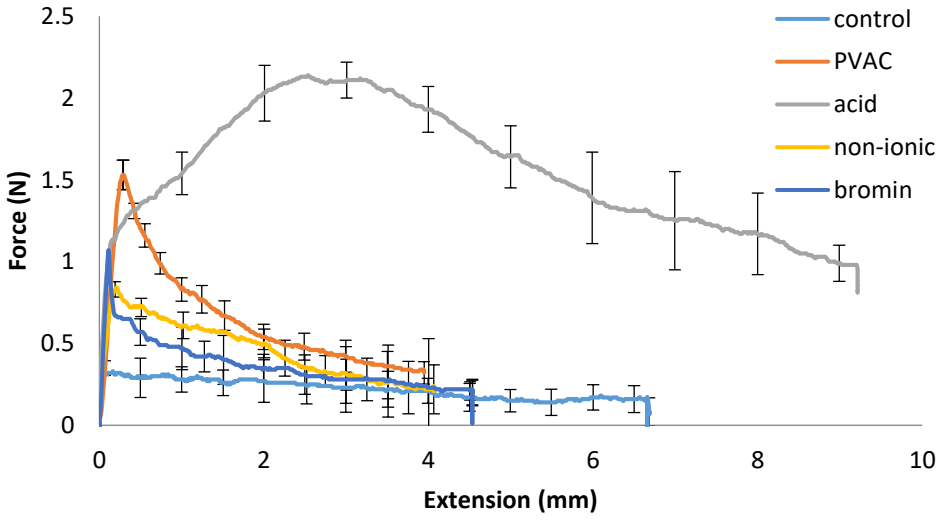

Fig. 3.8. Force-extension plots from single fiber pullout tests.

From the plots, it can be observed that initially the pullout force increases linearly with the applied load. After reaching to the peak load, the nonlinear region demonstrates the start of debonding from the cement matrix. Fiber-matrix interfacial crack growth is somewhat stable until the peak load is reached and then the crack growth becomes unstable. The crack growth continues with the increment of the pullout load and finally the fiber slips out of the matrix.

The discussed shear-lag theory was adopted to derive the bond strength and frictional bond between fiber-matrix interfaces. Three samples were used for each treatment case and the average values are reported. The results are tabulated in Table 3.3 to compare the effect of fiber treatment on fiber-matrix interface properties.

Table 3.3. Fiber-matrix interface properties extracted from single fiber pullout tests

Treatment Type	Average interfacial shear strength/standard deviation, τ (N/mm^2)	Average bond strength/standard deviation,τ_s (N/mm^2)	Average frictional bond/standard deviation, $\tau_{f,}$ (N/mm^2)
Untreated fiber	0.012/0.002	0.835/0.169	0.072/0.006
Bromine treatment	0.035/0.002	1.002/0.024	0.119/0.012
Non-ionic detergent Treatment Type	0.027/0.005	0.955/0.030	0.091/0.027
PVAC treatment	0.059/0.007	1.014/0.053	0.106/0.041
Acid treatment	0.007/0.003	1.040/0.042	0.134/0.032

From the fiber-matrix interface properties derived from single fiber pullout test, it is clear that the interface bonding is enhanced due to the chemical treatments. The acid treated fibers exerted the best interface bonding with more than five times of the average interfacial shear strength than that of untreated fibers. PVAC treatment also increased the average interfacial shear strength by almost five times.

3.3.3. Fiber Surface Roughness Test

The effect of the surface treatment on the Polypropylene fiber was also studied by examining the fiber surfaces with Atomic Force Microscopy (AFM). The AFM adopted is Veeco, Dimension 3100, which provides a high-resolution surface imaging with a sub-nm height-measurement capability in z direction and a tip-dependent x-y resolution. The treated fibers were carefully glued on glass slides to protect against any surface contamination. The cross-sectional area captured by the AFM was 20 µm x 20 µm as shown in Fig. 3.9. From Fig. 3.9, the surface topography change due to fiber treatment can be clearly seen in the image. Their corresponding surface roughness values calculated through the instrument software are shown in Fig. 3.10.

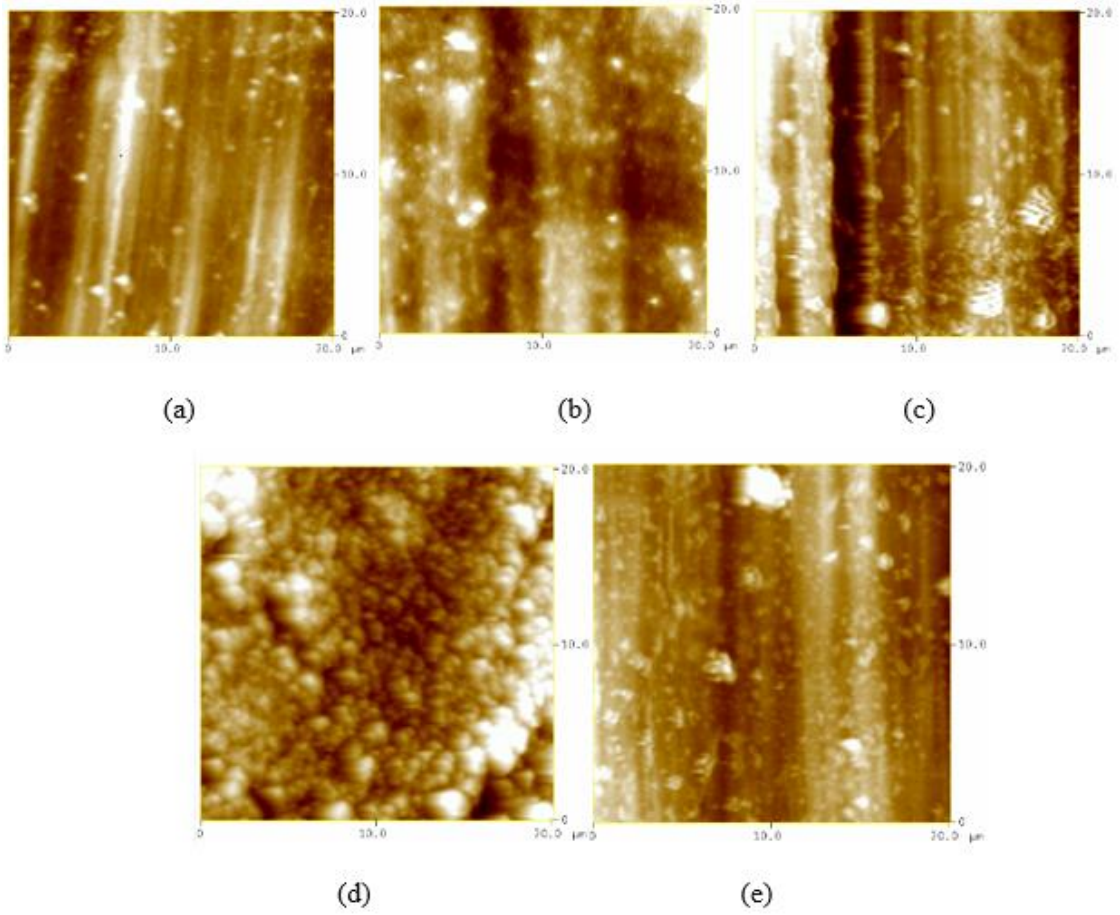

Fig. 3.9. AFM images of untreated and chemically treated polypropylene fiber surface (a) untreated fiber, (b) non-ionic detergent treated, (c) acid treated, (d) PVAC treated, and (e) bromine treated fiber.

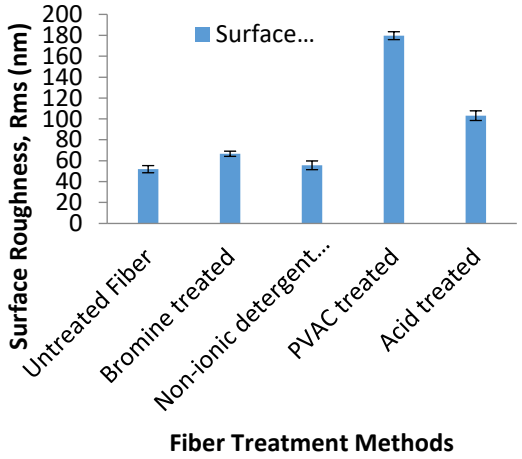

Fig. 3.10. Comparison of change in surface roughness due to chemical treatment

Fig. 3.10 shows that the fiber surface roughness has increased more than three times than that of untreated fibers due to PVAC treatment. The AFM image shows clear formation of PVAC coating on fiber surface which eventually leads to high surface roughness value. The acid treated fibers show a good increment in surface roughness values (close to 100%) as the acid peels off the top surface of the fiber and exposes the fibrillated portion. Acid also creates pores within the fiber surfaces which can be observed from the AFM images. The fibers with non-ionic detergent does not show an increment in RMS (Root Mean Square) value, as this type of treatment is conducted to increase the surface energy of the fiber, not the surface roughness.

3.3.4. Void Ratio Test

Void ratio tests were conducted for the pervious concrete cylinders. Three cylinders for each mix were tested and the average value is reported in Table 3.4.

Table 3.4. Void ratios of pervious concrete specimen (with 1% fiber)

Type	Void Ratio (%)	Standard deviation
Control Pervious concrete	20.71	0.53
With Untreated fiber	18.37	0.78
With Acid Treated fiber	17.95	0.44
With Detergent Treated fiber	18.11	0.27
With Polyvinyl Acetate (PVAC) treated fiber	18.07	0.16
With Bromine treated fiber	17.92	0.13

The void ratio results indicate that the void ratio of the pervious concrete is decreased by 1~3% with an addition of 1% fiber to the pervious concrete mix. Fiber addition during the mixing process tends to create a mesh like structure that involves the aggregates, cement paste and the fiber itself. Because of the high flexibility of polypropylene fibers, the void structure is reorganized and becomes more compact with the polypropylene fiber addition and thus results in a decreased void ratio.

3.3.5. Compression Strength Test

Three samples for each mix ratio were tested with the compression strength testing machine and the strength values were directly recorded from the test setup. The results are shown in Table 3.5.

Table 3.5. Compression strength of pervious concrete cylinders with treated and untreated fibers (1 ksi = 6.9 MPa)

Type	Compression Strength (ksi (MPa))	Standard deviation (ksi (MPa))
Control Pervious concrete	1.05 (7.24)	0.003 (0.020)
With Untreated fiber	1.06 (7.31)	0.11 (0.76)
With Acid Treated fiber	1.07 (7.38)	0.17 (1.17)
With Detergent Treated fiber	1.05 (7.24)	0.42 (2.90)
With Polyvinyl Acetate (PVAC) treated fiber	1.04 (7.17)	0.23 (1.59)
With Bromine treated fiber	1.06 (7.31)	0.46 (3.17)

The compression test result shows a very small increment (1~2%) due to the addition of polypropylene fibers to the pervious concrete specimen. The Acid treated fibers add a 2% more strength to the specimen, compared to that of pure pervious concrete. Because of high void content and low cementitious material, the bonding surface among fiber-aggregate-cement paste is limited. The addition of fiber thus has a little effect on the static compressive strength, rather the fiber contributes to the post cracking behavior and the moreover the ductility of the matrix. Fiber treatment can improve the existing bond between the fiber and matrix and thus can increase the compressive strength a little, but no significant improvement of compressive strength was observed through the study.

3.3.6. Flexural Strength Test

Modulus of rupture was tested and calculated for chemically treated and untreated PP fiber reinforced pervious concrete beam specimen as illustrated in Fig. 3.11. The results are shown in Table 3.6.

(a) (b)

Fig. 3.11. Beam specimen after flexural strength test (a) untreated PP fiber reinforced pervious concrete beam, (b) chemically treated PP fiber reinforced pervious concrete beam

Table 3.6. Modulus of rupture for chemically treated and untreated PP fiber reinforced beam specimen

Type	Peak load (kips (kN))	Modulus of rupture (psi (MPa))
Control Pervious concrete	4.55 (20.23)	365.51 (2.52)
	4.86 (21.64)	389.75 (2.69)
With Untreated fiber	4.98 (22.14)	423.51 (2.92)
	5.42 (24.11)	461.22 (3.18)
With Acid Treated fiber	6.28 (27.94)	512.90 (3.54)
	5.92 (26.35)	488.52 (3.37)
With Detergent Treated fiber	5.59 (24.88)	475.97 (3.28)
	5.64 (25.10)	465.28 (3.21)
With Polyvinyl Acetate (PVAC) treated fiber	5.78 (25.70)	486.53 (3.35)
	5.89 (26.22)	491.21 (3.39)
With Bromine treated fiber	5.35 (23.81)	457.80 (3.16)
	5.43 (24.16)	470.20 (3.24)

From Table 3.6, the experimental result shows that there is significant increment in flexural strength due to acid treatment (>30%) than that of pure pervious concrete. The acid treatment creates pores within the fiber that allows the cement matrix to bind stronger. Other treatment

methods show increment in flexural strength as well since the fiber surface roughness is increased due to the treatments (Fig. 3.12).

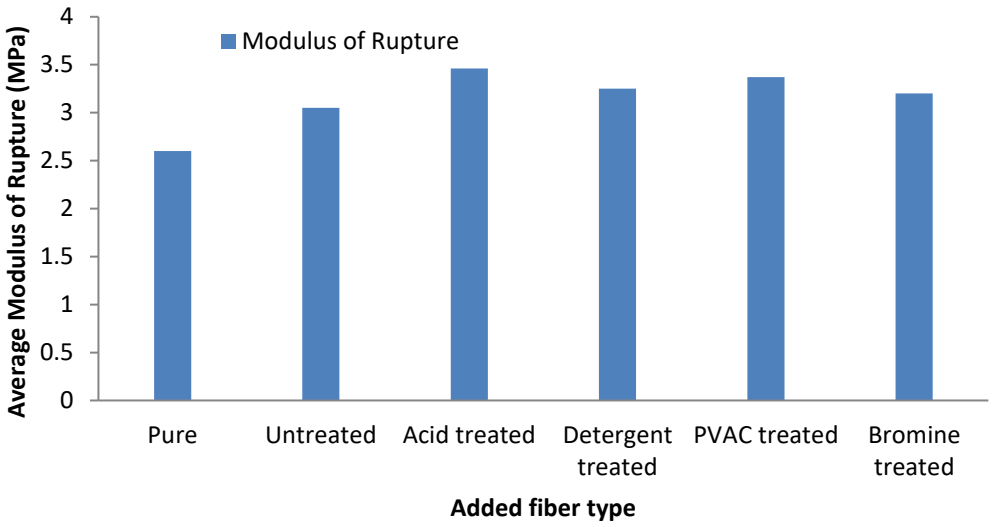

Fig. 3.12. Comparison of flexural strength between chemically treated and untreated polypropylene fiber reinforced pervious concrete specimen

3.4. Conclusion

Due to the presence of large number of pores, using fibers in pervious concrete to enhance its strength and stiffness remains a challenge for the researchers. Fibers treatment processes have increased the fiber surface roughness by either creating pores on the fibers or by adding a chemical coating, which could be a viable approach to overcome this challenge. Through a series of physical experiments, effect of using chemical treated polypropylene fibers as reinforcement in pervious concrete can be summarized as follows:

- Chemically treated fibers have shown higher bond strength with the concrete matrix and increased the flexural strength significantly for the pervious concrete samples tested. For instance, acid treated fibers have increased the flexural strength of pervious concrete more than 30% than that of pure pervious concrete, and more than 10% than that of untreated fiber reinforced pervious concrete.

- The interface bonding behavior of the fiber and cement matrix has been summarized as well and an increment of bond efficiency is reached through different chemical fiber treatments.
- Fiber-matrix interface properties determined through the fiber pullout test can be used in future research, such as finite element modeling and optimization of fiber reinforced pervious concrete.

The consistent experiment results in this paper have moved a step forward in the implementation of fiber reinforced pervious concrete. Further studies are still needed to explore the durability of polypropylene fiber reinforced pervious concrete.

3.5. References

[1] Aly T., Sanjayan J. G., and Collins, F. (2008). Effect of polypropylene fibers on shrinkage and cracking of concretes, Materials & Structures, 41(10), 1741–1753.10.1617/s11527-008-9361-2.

[2] ASTM C78/C78M-16, Standard Test Method for Flexural Strength of Concrete (Using Simple Beam with Third-Point Loading), ASTM International, West Conshohocken, PA, 2016, www.astm.org

[3] Carstens P.A.B., Marais S.A., Thompson C.J., (2000). Improved and novel surface fluorinated products, Journal of Fluorine Chemistry, 104, 97–107

[4] Darmanin T. and Guittard F., (2014). Wettability of conducting polymers: from superhydrophilicity to superoleophobicity, Progress in Polymer Science, 39, 656–682.

[5] Diehl D. and Schaumann G. E., (2005). Wetting kinetics determined from contact angle measurement, Geoohysical Research Abstracts, 7: 00414.

[6] Felix M.J. and Gatenholm P., (1991). The nature of adhesion in composites of modified cellulose fibers and polypropylene, Journal of Applied Polymer Science, 42, 609–20

[7] Fialova M., Moravek T., Kopkane D., Rahel J., Stahel P., and Cernak, M., (2012). Polypropylene Fibers modified by atmospheric pressure plasma as reinforcement for concrete, NANOCON, Brno, Czech Republic, EU.

[8] Fischera G. and Li, V. C., (2007). Effect of fiber reinforcement on the response of structural members, Engineering Fracture Mechanics, 1-2, 258-272.

[9] Hannat D. J., (1978). Fiber Cements and Fiber Concretes. John Wiley and Sons, Inc., New York

[10] Kevern J., Wang K. M., Suleiman M., and Schaefer V., (2005). Mix Design Development for Pervious Concrete in Cold Weather Climates, Paper presented at the Mid-Continent Transportation Research Symposium, Ames, IA.

[11] Kopczynska A., Ehrenstein G.W., (2007). Polymeric surfaces and their true surface tension in solids and melts, Journal of Materials Education, 29, 325–40.

[12] Laws V., Lawrence P., and Nurse R. W., (1972). Reinforcement of brittle matrices by glass fibers, Journal of Physics, D: Applied Physics, 6: 523-537.

[13] Lundquist L., Marque B., Hagstrand P.O., Leterrier Y., and Manson J.A.E., (2003). Novel pulp fiber reinforced thermoplastic composites, Composite Science and Technology, 63,137–52

[14] Martínez-Barrera G., Vigueras-Santiago E., Hernández-López S, MenchacaCampos C, Brostow W., (2005). Mechanical improvement of concrete by irradiated polypropylene fibers, Polymer Engineering & Science, 45, 1426–31.

[15] Mohanty A.K., Drzal L.T., and Misra M., (2002). Engineered natural fiber reinforced polypropylene composites: influence of surface modifications and novel powder impregnation processing, Journal of Adhesion Science & Technology, 16, 999–1015

[16] Mohebby B., Ghotbifar A., Kazemi-Najafi S., (2011). Influence of maleic anhydride polypropylene (MAPP) on wettability of polypropylene/wood flour/glass fiber hybrid composites, Journal of Agricultural Science and Technology, 13: 877-884.

[17] Mora-Ruacho J., Gettu R., and Aguado A., (2009). Influence of the shrinkage-reducing admixtures on the reduction of plastic shrinkage cracking in concrete, Cement & Concrete Research, 39 (3), 141–146.

[18] Orchon S., (1958). Wetting angle determinations – A tool for evaluation of coating adhesion, TAPPI, 41(1): 33-37.

[19] Peled A. and Mobasher B., (2005). Pultruded fabric-cement composites, ACI Material Journal, 1, 10215–23.

[20] Peled A., Guttman H., and Bentur A., (1992). Treatment of Polypropylene fibers to optimize their reinforcing efficiency in cement composites, Cement and Concrete Composites, 4, 14277-85.

[21] Sheldon R. P., (1982). Composite Polymeric Materials, Applied Science Publishers, New York, p. 85.

[22] Zafeiropoulos E.N., Baille C.A., and Hodgkinson, J.M., (2002). Engineering and characterization of the interface in flax fiber/polypropylene composite materials: Part II. The effect of surface treatments on the interface, Composites: Part A, 33, 1185–90

[23] Zhang C., Gopalaratnam V.S., and Yasuda, H.K., (2000). Plasma treatment of polymeric fibers for improved performance in cement matrices, Journal of Applied Polymer Science, 76, 1985–1996

[24] Zheng Z., Feldman D. (1995). Synthetic fiber-reinforced concrete, Progress in Polymer Science, 20, 185–210.

CHAPTER 4. MICROMECHANICAL MODELING OF PERVIOUS CONCRETE REINFORCED WITH TREATED FIBERS

4.1. Introduction

Pervious concrete has been widely used in parking lots and airport fields. However, excessive cracking and spalling issues of pervious concrete remains a challenge for adopting them in wider applications, as the binding material proportion is low, and the use of fine aggregates is nearly zero. When loading in compression, the failure appears first in the weak concrete zone induced by the random distribution of voids. The process continues until the failure of the whole specimen occurs. Fiber reinforcement delays the crack generation and enhances the strength of the host matrix. However, the bonding mechanism between fiber & concrete matrix is controversy in literature and needs better explanation. In this work, the influence of polypropylene fiber inclusion on the strength and stiffness of pervious concrete microstructure is studied through delicate interface modeling. 2D microstructures of pervious concrete were generated using MATLAB and ANSYS parametric design language (APDL). Cohesive zone technique has been used to model the interface between fiber and concrete matrix. Load-displacement plots were generated in ANSYS for specimen under compression for varied void-fiber percentages and different treated interface properties. In such sense, the developed micromechanical model provides a useful tool to develop optimal fiber reinforced pervious concrete.

Microstructure of concrete, specially the pore structure, controls the mechanical properties of concrete. A well-controlled pore structure has been seen to improve the properties of fresh portland cement concrete (Li et al., 2007), hardened and cured concrete (Cheeseman et al., 2005), and to enhance the concrete durability (Hassan et al., 2010). Fibers are widely used in concrete to enhance its properties as well. The most commonly used fibers are steel fibers, polypropylene

fibers and fiberglass fibers. In most cases, fibers are randomly distributed. Cracking of the brittle matrix composites like concrete is generally initiated at a dominant fracture or void space of the section created while mixing. Once a crack is formed within a fiber reinforced concrete matrix, the bridging fibers across the crack determine the load carrying capacity of the composite. Thus, performance of the composite is largely governed by random distribution of fibers, fiber volume, fiber orientation, and void distribution in the cementitious matrix.

Polypropylene fibers are cheap and often used in in overlays and pavements, slabs, flooring systems, and precast pile shells to overcome the surface crack problem (Alhozaimy et al., 1996). Researches also showed that adding fibers to a concrete matrix increases the bending strength and formability of the matrix. Polypropylene fibers could also improve spalling behavior of concrete (Zeim et al., 2006). Due to its high tensile and pull-out strength, the polypropylene fibers even reduce the early plastic shrinkage cracking by enhancing the tensile capacity of fresh concrete (Banthia et al., 2006). Due to these reasons, polypropylene fiber reinforced pervious concrete is the focus of this paper.

The surface smoothness and inert chemical nature of commercially available polypropylene fibers affect the bonding between the fiber-concrete interface. The hydrophobic nature and the low surface energy of Polypropylene fiber led to lower fiber-matrix bond strength. Chemical treatment of polypropylene fibers can increase the surface roughness, porosity and surface energy, thus offers a better fiber-matrix interface bonding.

A significant number of finite-element (FE) models have been developed to date to predict the nonlinear behavior of fiber reinforced concrete composites under static and dynamic loading. The analytical formulation of such models is generally based on the combined use of relevant experimental data and continuum mechanics theories (Abbas et al., 2016) such as nonlinear

elasticity, plasticity, visco-plasticity and damage mechanics. The formulation of such models is described by several parameters, and the evaluation of these parameters is essential to achieve close correlation between the numerically predicted nonlinear specimen behavior and the experimentally obtained data. These parameters are usually associated with post-failure concrete behavior such as strain softening, tension stiffening, shear-retention ability etc. Their values are often established through calibration based on the use of experimental information at the structural level, rather than at the material level (Kotsovos et al., 2008). The use of such parameters tends to unleash the ductile characteristics to plain concrete behavior, which are not compatible with its brittle nature. Thus, they cannot be justified by the relevant test data. As a result, the numerical predictions are affected and require recalibration to match with the actual cases (Kotsovos et al., 2009). Moreover, the use of such models is considered generally too complicated for practical applications. The results obtained are not always accepted to be reliable.

As summarized by the above literature review, fiber reinforcement enhances the properties of pervious concrete, but there are no accurate existing finite element tools that could capture its behavior. In this study, a micromechanical model of polypropylene fiber reinforced pervious concrete is studied through delicate fiber-bonding-interfaces. 2D concrete microstructure is first generated through MATLAB and meshed through the ANSYS Parametric Design tool. The voids and the fibers are distributed randomly over the matrix with a control of void and fiber volume fraction. Fiber-matrix interfaces are modeled as cohesive zone elements and their properties were extracted from the single-fiber pullout tests of chemically treated polypropylene fibers. The three-phase microstructure is then analyzed under compression loading and load-displacement plots are generated. Thus, the developed micromechanical model provides a useful tool to optimize the mechanical properties of fiber reinforced pervious concrete.

4.2. Characterization of Interface Behavior Through Single Fiber Pull-Out Tests

4.2.1. Bilinear Cohesive Zone Model

Properties of the fiber-matrix interphase in composites have a significant influence on their structural performance. Li et al. (2005) presented a cohesive-zone model for a fiber-reinforced polymer–matrix composite. To define the fracture of notched or cracked specimens, the authors proposed a two-parameter model with characteristic toughness and strength. The parameter values were determined through a fracture test, by making comparison of the experimental outcome to the numerical predictions. The study concludes that the use of cohesive zone model can be beneficial to predict the transition between catastrophic and stable crack growth in a composite. Subramani et al. (2013) adopted cohesive zone modeling approach to simulate the crack propagation and interphase failure for an E-glass fiber-epoxy system. The cohesive zone model parameters were derived from the numerical simulations based on the lab experiment results for the composite. Park et al. (2010) proposed a constitutive model for cohesive fracture of fiber reinforced concrete by differentiating the aggregate bridging zone and the fiber bridging zone. Three-point bending and splitting tensile tests were conducted, and fracture parameters were extracted from the results. The parameters of the cohesive fracture model were then defined by the outcome of the experimental results. The proposed model explains the fracture behavior of plain concrete beams and also can be used to predict the fracture behavior of fiber reinforced concrete beams.

ANSYS implemented the cohesive zone model through its Cohesive Zone Modeling (CZM) tool, which could be used to simulate the bonding and debonding behavior of interfaces between fiber and matrix. The interface properties could be extracted from the single fiber pullout

test from cement matrix and then used to mimic the pullout force-extension behavior for each treatment case.

ANSYS allows two types of interface models to be used directly through the APDL command, bilinear & exponential behavior. In this study, mode II bilinear behavior is adopted to simulate the cohesive zone along the fiber and matrix interface.

Mode II dominated bilinear CZM model assumes that separation of material interfaces is controlled by the tangent displacement jump of the interface (Alfano et al., 2001), which is shown in Fig. 4.1.

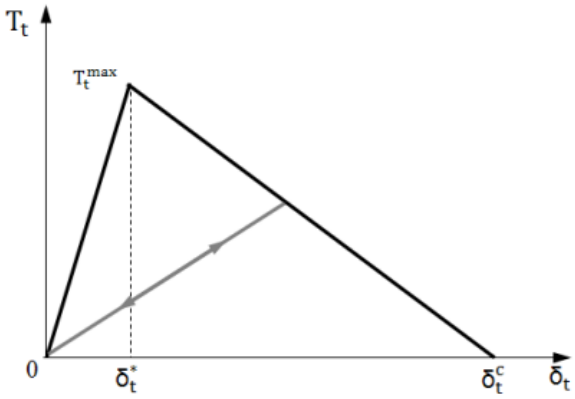

Fig. 4.1. Bilinear mode II dominated cohesive zone model

In Figure 4.1, T_t^{max} stands for the maximum tangential traction, δ_t* is the tangential displacement at maximum traction, and δ_t^c is the tangential displacement at the completion of debonding.

4.2.2. Single Fiber Pullout Test

Single fiber pullout test is one of the most commonly used techniques to characterize the fiber-cement matrix interface properties. In this study, single fiber pullout tests have been carried out for treated and untreated polypropylene fibers. The fiber used in this test is 19 mm in length with a diameter of 0.76 mm. The fiber embedded length was controlled at 12 mm.

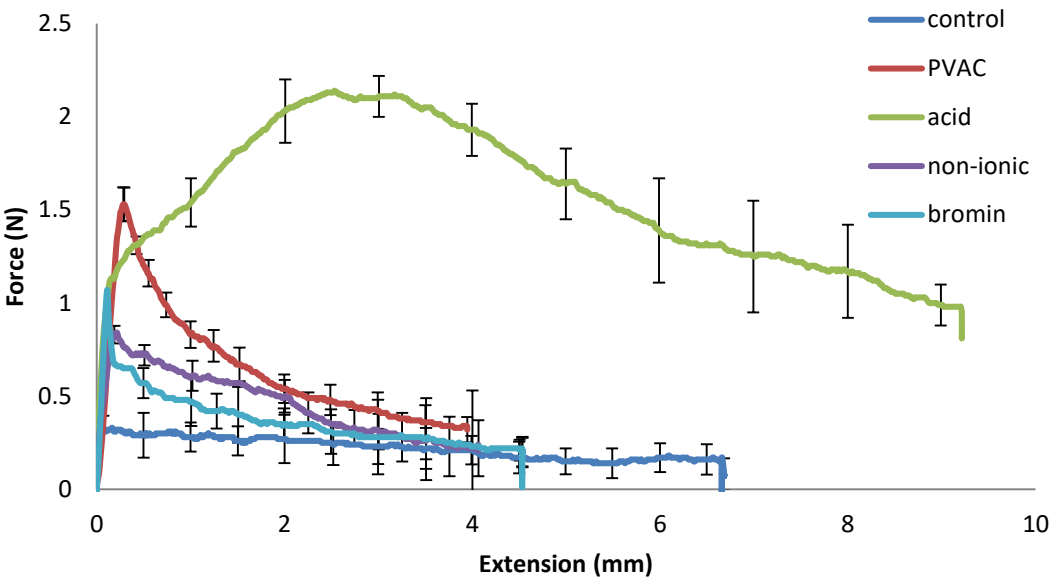

Fig. 4.2. Force-extension plot from single fiber pullout test

Force-displacement plots were generated through the single fiber pullout test of untreated and chemically treated fibers as shown in Fig. 4.2. Since the force-displacement behavior of the experimental analysis is not exactly bilinear, the cohesive zone parameters were extracted in two different ways, case 1: linear interpolation through the peak and the initial slope of the debonding zone and case 2: linear interpolation through peak and end failure point (Fig. 4.3). Case 1 describes the most brittle post-peak behavior, while case 2 captures the most ductile post-peak behavior. Any real responses of the fiber reinforced pervious concrete will lie in between these two cases. Based on the experimentally derived force-displacement plots in Fig. 4.2, the predicted cohesive zone parameters are listed in Table 4.1.

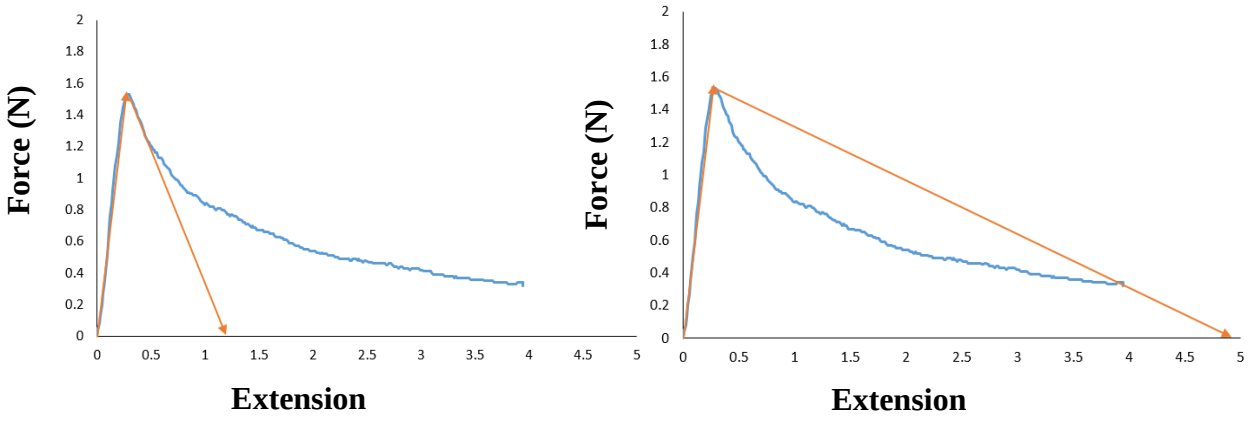

(a) (b)

Fig. 4.3. Extraction of cohesive zone model parameters from single fiber pullout test results (a) Linear interpolation through peak and initial softening slope (b) Linear interpolation through peak and end failure point.

Table 4.1. Predicted cohesive zone parameters from single fiber pullout tests for different treatment cases.

Treatment Type	Maximum tangential traction (N)	Tangential displacement at maximum traction (mm)	Tangential displacement at the completion of debonding (mm)	
			Linear interpolation through peak and initial softening slope	Linear interpolation through peak and end failure point
Untreated fiber	0.162	0.15	0.3	6.4
Bromine treatment	1.07	0.2	0.4	5.5
Non-ionic detergent Treatment Type	0.84	0.2	1.3	5.6
PVAC treatment	1.52	0.275	1.1	5
Acid treatment	2.12	2.5	5.6	10.5

4.2.3. Single Fiber Pullout Simulation in ANSYS

The extracted bilinear mode II cohesive zone parameters are then used to simulate the single fiber pullout test in ANSYS. A 2D cement matrix is generated in ANSYS with dimension of 1 x 1 in (25 x 25 mm). The fiber embedded length is taken as 12 mm and the fiber length and diameter is kept at 19 mm and 0.76 mm respectively (same as the experimental setup). The cement matrix material properties are adopted from the experimental study by Leung et al. (1999). The combined fiber and cement matrix properties are listed in Table 4.2.

Table 4.2. Material properties of polypropylene fiber and cement matrix

	Elastic modulus, GPa	Poisson's ratio	Compressive Strength, MPa
Polypropylene Fiber	4	0.38	-
Cement Matrix	30	0.2	36.5

A given displacement is applied at the fiber right end (Fig. 4.4), with a standard loading rate of 2 mm/min. The force-displacements derived from the fiber pullout simulation were extracted and shown in Fig. 4.5.

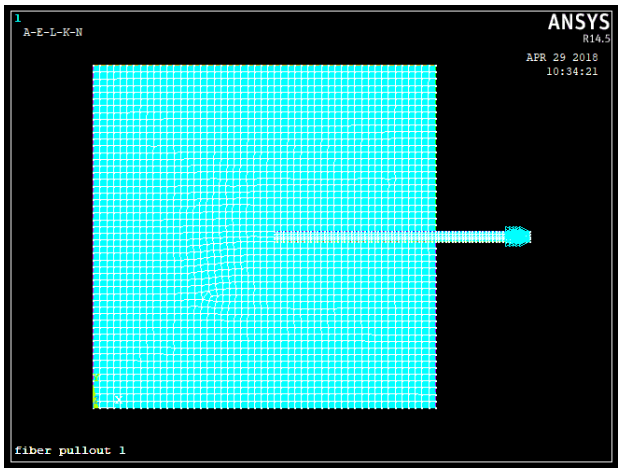

Fig. 4.4. Single fiber pullout test in ANSYS

4.2.4. Comparison Between ANSYS and Experimental Results

Fig. 4.5 shows the comparison between the force displacement behavior of experimental and ANSYS simulation of the fiber pullout test. The comparison is made for all the treatment cases and tabulated in Table 4.3.

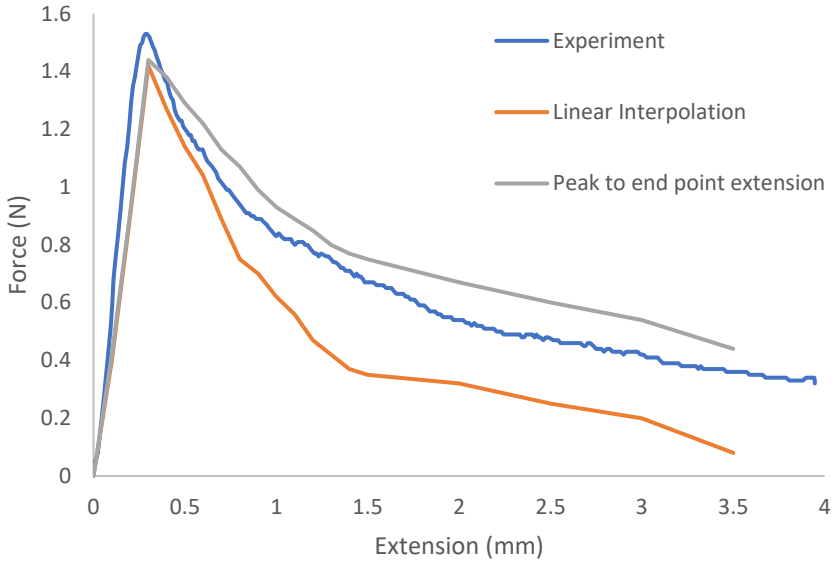

Fig. 4.5. Comparison of force extension plot for PVAC treated fibers

Table 4.3. Comparison of force-extension behavior of the experimental and simulated fiber pullout tests

Treatment type	Peak force (N)			Slope of pre-peak region		
	Experiment	Case 1	Case 2	Experiment	Case 1	Case 2
PVAC treated	1.52	1.42	1.44	5.85	4.80	4.83
Acid treated	2.12	2.10	2.18	0.53	1.02	1.05
Bromine treated	1.07	0.90	1.02	9.95	9.56	10.21
Non-ionic detergent treated	0.84	0.77	0.80	4.16	3.90	4.05

From Fig. 4.5 and Table 4.3, it can be seen that the peak forces and the slopes of all specimens are well captured, when compared to the experimental data. Since the different treatment processes affect the polypropylene fibers differently, the slope of the pre-peak region of the force-extension diagram varies within a certain region. The acid treated fibers possess the most strength to the fibers and hence the slope of the pre-peak region stays low. The numerical results fall within good accordance to the experimental results, capturing the fiber-matrix interface debonding.

4.3. Generation Of 2D Microstructure of Fiber Reinforced Pervious Concrete

Fiber reinforced pervious concrete has three phases: voids, fibers, and concrete matrix. Random distribution of fiber and void was generated in MATLAB, where fibers were designated as ellipses (considering its large longitudinal dimension) and voids were assigned as circular shapes. The dimension of the matrix was kept as 100 x 100 mm (4 x 4 in). The void percentage was varied from 15% to 20% and the fiber percentage was varied in between 1% to 3% (Fig. 4.6).

Area masking technique was used to ensure no overlapping of fibers and voids. Then the generated microstructure was transferred to ANSYS and a block of 2D geometry of fiber reinforced pervious concrete has been created. Finite element analysis was then conducted on the microstructure model through the derived microstructure characteristics using ANSYS Parametric Design Language (APDL).

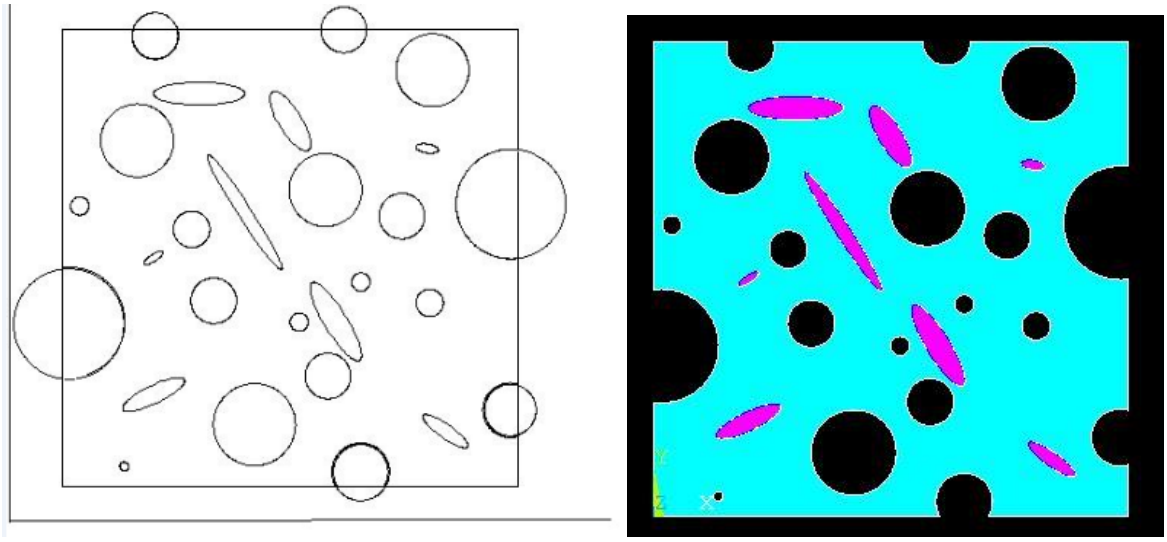

(a) (b)

Fig. 4.6. (a) Generated 2-D microstructure (100 mm x 100 mm) in MATLAB with 15% void and 1% fiber (b) Microstructure generated in ANSYS with boundary cut-offs.

To model the fiber-matrix interface, Cohesive Zone Modeling (CZM) technique was used. Bonded contact method with general surface to surface contact was adopted. The CZM model consists of a constitutive relation between the traction acting on the interface and the corresponding interfacial separation. Three material models were used to define the fiber-matrix interface, INTER203, CONTA172 and TARGE169 (Fig. 4.7).

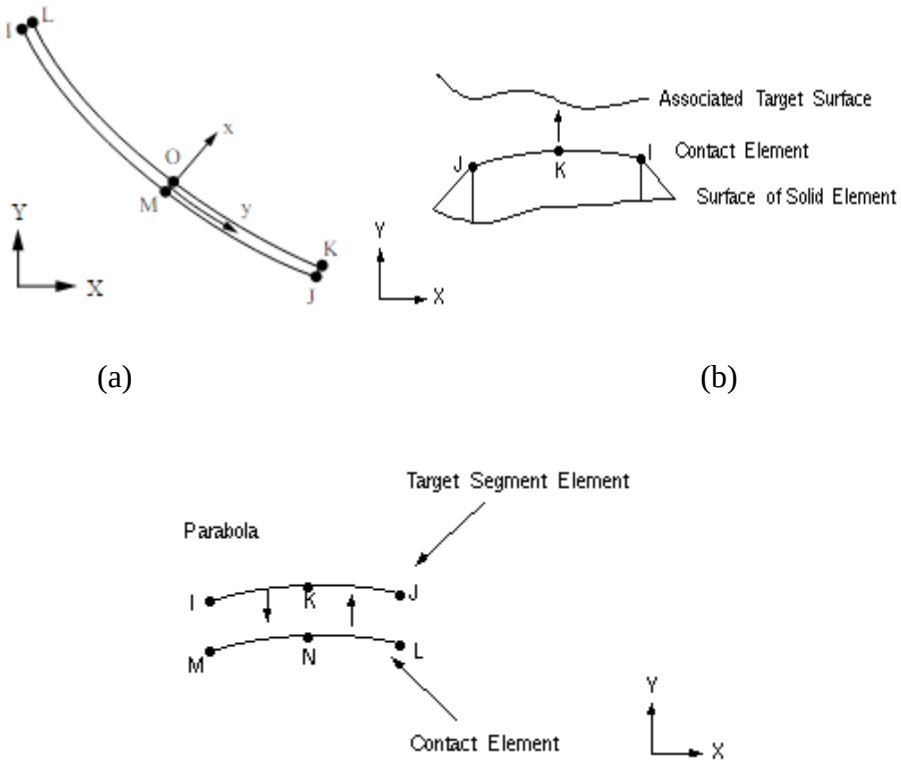

Fig. 4.7. Geometry of (a) INTER203 (b) CONTA172 and (c) TARGE169 elements

The contact and target elements were assigned to concrete matrix and fiber surface respectively. Then the cohesive zone was defined with interface elements, in this case with INTER203.

4.4. Load Deflection Analysis of Fiber Reinforced Pervious Concrete

To model the specimen in ANSYS, element type of PLANE183 is used. This element type is defined by 8 nodes or 6 nodes having two degrees of freedom at each node: translations in the nodal x and y directions. The boundary condition was chosen as a roller support at the bottom surface and fixed at the middle point of that surface. A uniaxial compression simulation is conducted for the generated microstructure model with a displacement-controlled boundary condition. The thickness of the section is taken as unity. Displacement stroke was applied to the

top surface and the other two sides were kept as free. The applied displacement deforms the model, initiates cracks and failure in the concrete matrix. Maximum strain failure criterion is currently selected for this case (Fig. 4.8).

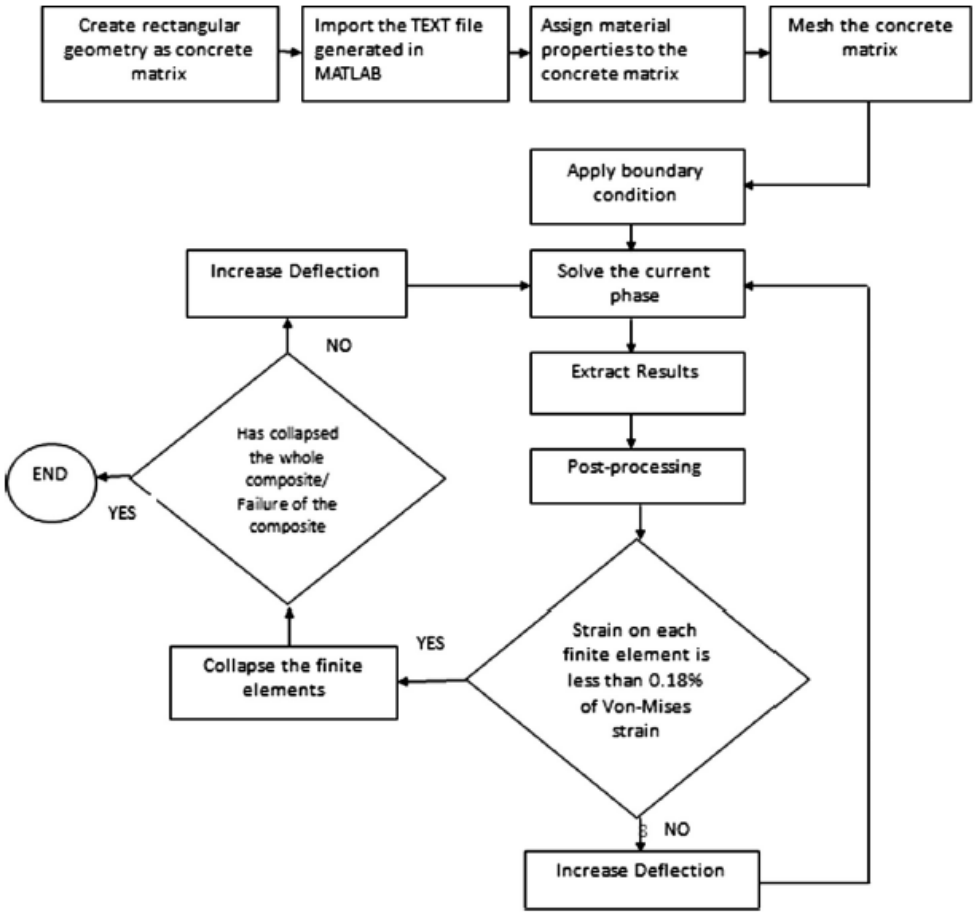

Fig. 4.8. Flow chart for ANSYS analysis of failure in pervious concrete

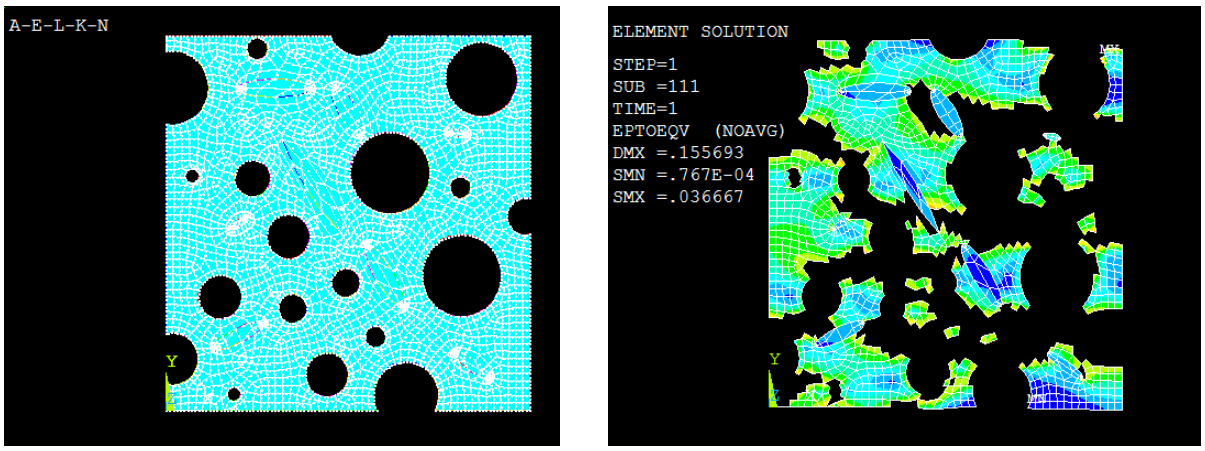

(a) (b)

Fig. 4.9. (a) Meshed microstructure with cohesive zone applied to fiber-matrix interface (b) Von-Mises strain plot after failure

ANSYS postprocessing was used through APDL to simulate the progressive failure. The model elements were inspected with respect to maximum strain and the 'EKILL' command was used to eliminate the elements that surpassed the maximum strain. The remaining geometry went through deflection-controlled loading and this loop continued until the whole matrix is collapsed. Fig. 4.9 shows a test case with a fiber-reinforced pervious concrete matrix with 15% void and 1% fiber. The composite matrix dimension is taken as 100 x 100 mm. The size of generated fibers was controlled between 0~19 mm.

The displacement-controlled loading eventually leads to a total matrix failure. The crack initiates from the tip of voids and propagates through the matrix. Cracks are arrested in the fiber surface and no fiber failure or fiber full debonding is observed in this case. The crack connects the voids and reaches to a crack-through failure.

4.5. Parametric Study

4.5.1. Effect of Fiber Volume Fraction

The ANSYS model was further simulated with varied void percentages and fiber volume fractions, and with different fiber treatments. The void ratio was varied from 15-20% and the fiber volume fraction was varied in a range of 1-3%. The strength and stiffness of the composite matrix is obtained through the ANSYS post-processing analysis and then normalized with respect to their highest values. A normalized strength and stiffness thus defined could be calculated as,

$$\frac{\text{Stiffness}}{\text{Highest stiffness from all treatment cases}} + \frac{\text{Strength}}{\text{Highest strength from all treatment cases}}.$$

For four different treatment cases, the effect of fiber volume fraction on the normalized strength & stiffness is shown in Fig. 4.10.

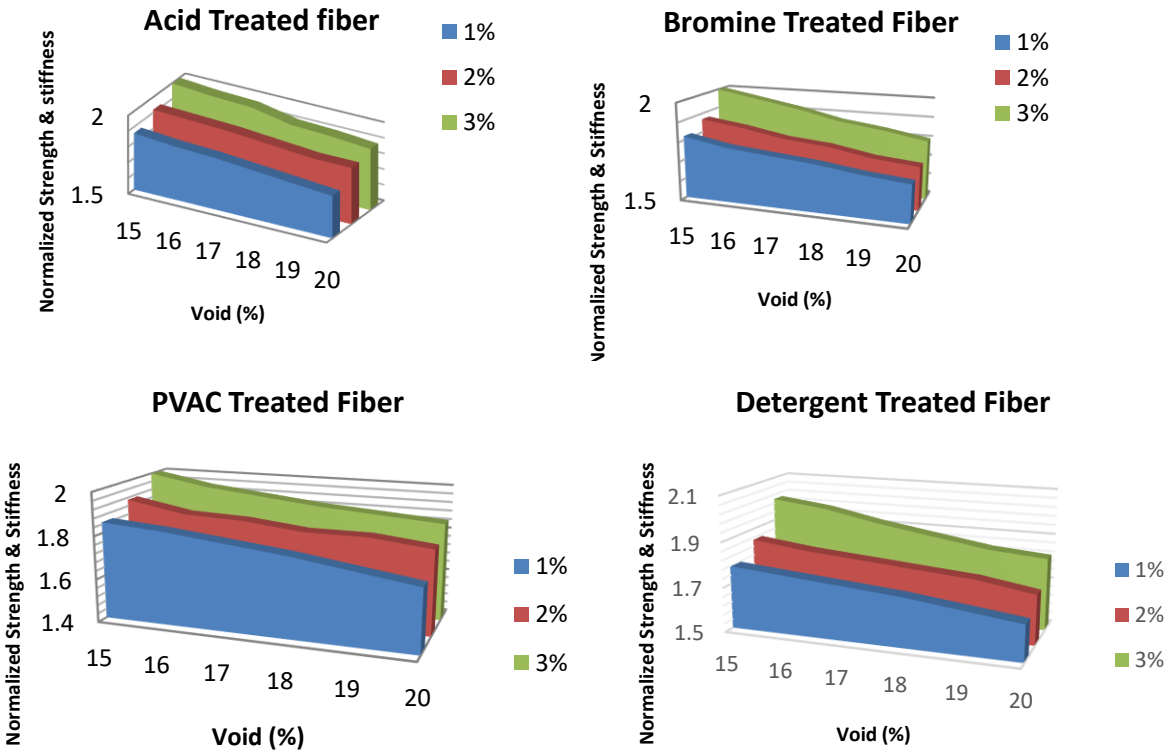

Fig. 4.10. Effect of fiber volume percentages on strength and stiffness for different treatment cases.

From the results shown in Fig. 4.10, a fiber volume of 3% and void ratio of 15% provides the highest strength and stiffness for all the treatment cases.

4.5.2. Effect of Interface Parameters

To study the effect of fiber-matrix interface parameters due to different fiber treatment processes, the 2D ANSYS model was simulated with varied void and fiber percentages. Fig. 4.11 shows the comparison of the effects of fiber-matrix interface parameters on strength and stiffness for 15% void and 3% fibers.

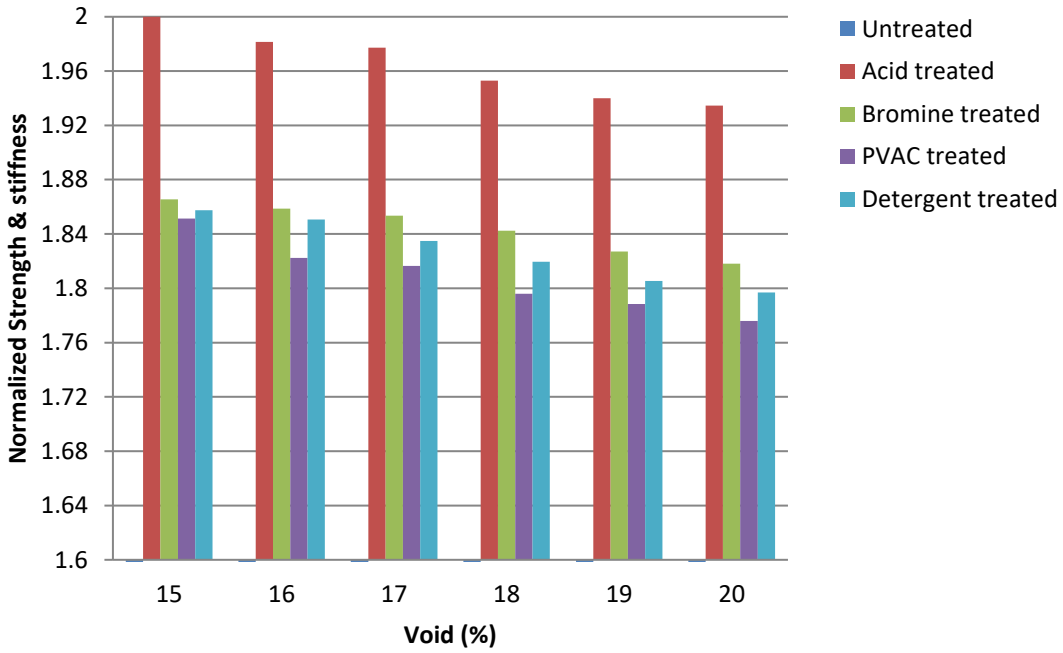

Fig. 4.11. Effects of different treatment processes on the normalized strength and stiffness (microstructure with 15% void and 3% fiber)

From Fig. 4.11, it could be seen that a significant improvement on strength and stiffness is attributed to the interface properties enhanced through the acid treated fiber.

4.6. Conclusions

In this study, bilinear cohesive zone model is adopted to simulate the interface of treated fiber and matrix interface. The cohesive zone model parameters were extracted from single fiber pullout tests. The derived cohesive zone parameters were then used to simulate the single fiber pullout test in ANSYS to validate the pullout model. With the validated cohesive zone model, fiber reinforced pervious concrete models are generated through MATLAB and ANSYS and simulated under displacement-controlled compression loading. To simulate a simplified microstructure, it was assumed that the fibers are parabolic in shape and the voids do not overlap with the fibers within the matrix. Resulting stress-strain plots were generated. The effect of fiber volume fraction and the effect of interface properties on fiber reinforced pervious concrete stiffness and strength were tabulated and compared with each other. Instead of assuming perfect bonding between fiber and matrix, the suggested model uses the interface properties obtained through fiber pullout tests, which provides an accurate tool to optimize the fiber reinforced pervious concrete.

4.7. References

[1] Li X., Bertos M., Hills C., Carey PJ., Simon S., (2007). Accelerated carbonation of municipal solid waste incineration fly ashes. Waste Manage, 9:1200–6.

[2] Cheeseman CR, Makinde A, Bethanis S., (2005). Properties of lightweight aggregate produced by rapid sintering of incineration bottom ash, Resources, Conservation and Recycling, 4, 147-162.

[3] Hassan M., Khalid H., (2010). Mechanical and environmental characteristics of bituminous mixtures with incinerator bottom ash aggregates. International Journal of Pavement Engineering, 11:83–94.

[4] Alhozaimy A.M., Soroushian P., Mirza F., (1996). Mechanical properties of polypropylene fiber reinforced concrete and the effects of pozzolanic materials, Cement and Concrete Composite, 18(2), 85-92.

[5] Zeim M., Leithner D., Lackner R., Mang H.A., (2006). How do polypropylene fibers improve the spalling behavior of in-situ concrete?, Cement and Concrete Research, 36(5), 929-942.

[6] Banthia N., and Gupta R., (2006). Influence of Polypropylene fiber geometry on plastic shrinkage cracking in concrete, Cement and Concrete Research, 36, 1263-1267.

[7] Abbas A.A., Mohsin S.M.S., Cotsovos D.M., (2016). A simplified finite element model for assessing steel fibre reinforced concrete structural performance, Computers and Structures, vol. 173, pp. 31–49. DOI: 10.1016/j.compstruc.2016.05.017.

[8] Kotsovos M.D., Pavlović M.N., Cotsovos D.M. (2008). Characteristic features of concrete behavior: Implications for the development of an engineering finite element tool, Computers and Concrete, 5(3), 243–260.

[9] Cotsovos D.M., Zeris C.A., Abbas A.A., (2009). Finite element modelling of structural concrete, Proceedings of the International Conference on Computational Methods in Structural Dynamics COMPDYN 2009, Rhodes, 22-24 June 2009.

[10] Li S., Thouless M.D., Waas A.M., Schroeder J.A., Zavattieri P.D., (2005). Use of a cohesive-zone model to analyze the fracture of a fiber-reinforced polymer–matrix composite, Composites Science and Technology, 65, 537–549.

[11] Subramani S., Gillespie John., Keef M., (2013). Detailed modeling and analysis of single fiber microdroplet test using cohesive zone approach. International SAMPE Technical Conference. 765-774.

[12] Park K., Paulino G., Roesler J., (2010). Cohesive fracture model for functionally graded fiber reinforced concrete. Cement and Concrete Research, 40(6), 956-965.

[13] Alfano G., Crisfield M., (2001). Finite element interface models for the delamination analysis of laminated composites: mechanical and computational issues. International Journal of Numerical Methods in Engineering, 50 (7), 1701–1736.

[14] Leung C. K. Y. and Shapiro N., (1999). Optimal steel fiber strength for reinforcement of cementitious materials, Journal of Materials in Civil Engineering 112: 116–123.

CHAPTER 5. OPTIMIZATION OF FIBER REINFORCED PERVIOUS CONCRETE

5.1. Introduction

Many classical approaches were developed in literatures to predict the material properties of a composite material including Hashin-Strikman method (Hashin Z., 1962), Mori-Tanaka principle (Mori et al., 1973) and self-consistency approach (Hill R., 1965), in which the fiber inclusion percentage and their distribution have shown dominant effects. Over the years, researchers have given significant efforts to inspect, improve and quantify the uniform distribution of reinforcing fibers in cementitious matrices (Woo et al., 2005, Lee et al., 2009, Yan et al., 2009). Ghashemi et al. (2014) studied the distribution of fiber in fiber reinforced composite by using NURBS functions. A function to describe the fiber dispersion was defined in the study and gradient based optimization method has been adopted. The method can lead to reach the optimum condition with smooth convergence. Brighenti et al. (2005) optimized the distribution of fiber in fiber-reinforced matrix using genetic algorithm and later developed a micromechanical model explaining the reinforcing distribution optimization approach. The researchers then discussed the reliability of the design of material composition by comparing with expected optimum conditions. The aim of these studies was to find equivalent material characteristics from a representative volume element. The fiber reinforced concrete constitutive behavior was evaluated by evaluating the stress distributions along the fiber-matrix interface while load is applied.

The inclusion of fiber into pervious concrete adds a few new variables to the optimization of such materials. As pervious concrete features a void percentage of 15~20%, the role of void is significant on the optimization processes. Optimization of the fiber reinforced pervious concrete needs attention to the parameters of void percentages, fiber percentages, and fiber-matrix interfacial properties. This chapter investigates two simplified but efficient optimization processes,

response optimization using desirability function and optimization through overlaid contour plots, to reach the desired strength and stiffness of pervious concrete. The generated finite element model through ANSYS and MATLAB is used to create a database of strength and stiffness of fiber reinforced pervious concrete matrices by varying fiber and void percentages. Fiber matrix interface properties extracted from single fiber pullout test is used in the model to define the interface behavior. The extracted database from the model is then used to optimize the fiber reinforced pervious concrete to reach to a certain range of desired strength and stiffness.

5.2. Optimization Techniques

Optimization of polypropylene fiber reinforced pervious concrete is performed using the strength and stiffness results obtained from ANSYS model. The model was generated with void percentages varying in between 15-20% and fiber percentages in between 1-3%. Fiber-matrix interface properties extracted from fiber pullout test for four different fiber treatment processes were used to define the fiber-matrix interfaces of the model. The interface properties include maximum tangential traction, displacement at maximum traction and displacement at debonding.

The response optimization technique identifies the combination of variable settings that collectively optimize a single response or a set of responses. MINITAB Response Optimizer tool is used to optimize the effect of void percentage, fiber percentage and different treatment techniques on the strength and stiffness of the fiber reinforced pervious concrete.

There are two approaches to optimize multiple response optimization. The first approach is the desirability function method. For problems associated with multiple response, desirability function method is widely used by researchers. The desirability function method transforms the response variable to reach a desirability value. The desirability value is proportional to the importance given to the individual response variables. This approach identifies the weight and

priority of the response variable to optimize the system. The desirability approach estimates the multiple response functions as polynomial functions of response variables.

The second approach is the influence envelope for multiple responses. In this method, each response function is optimized individually, and the contour plots are superimposed on each other to find the region where the solution lies. Then the optimal location is identified visually.

Table 5.1 shows the generated database from ANSYS model for acid treated fiber reinforced pervious concrete. Simulations through ANSYS model was performed by varying the void percentages from 15~20% and fiber percentages from 1~3%. The strength and stiffness results extracted from the ANSYS simulation, each value was obtained from the average of three simulations.

Table 5.1. Database generated from ANSYS model for treated fiber reinforced pervious concrete

Void (%)	Fiber (%)	Strength (MPa)	Stiffness (MPa)	Normalized Strength	Normalized Stiffness	Normalized strength and stiffness
	1	9.71	239.97	0.91	0.95	1.86
15	2	10.31	240.78	0.95	0.97	1.92
	3	10.79	250.45	1.00	1	2
	1	9.60	237.88	0.89	0.95	1.84
16	2	10.26	238.94	0.96	0.95	1.91
	3	10.63	248.22	0.99	0.99	1.98
	1	9.55	236.02	0.89	0.94	1.83
17	2	10.24	238.09	0.94	0.95	1.89
	3	10.61	247.69	0.99	0.98	1.97
	1	9.32	235.93	0.86	0.95	1.81
18	2	10.12	236.60	0.93	0.95	1.88
	3	10.22	244.93	0.95	0.97	1.92
	1	9.23	235.17	0.85	0.94	1.79
19	2	9.92	236.37	0.92	0.94	1.86
	3	10.11	243.28	0.93	0.96	1.91
	1	9.00	234.60	0.84	0.93	1.77
20	2	9.87	235.79	0.92	0.94	1.86
	3	9.96	242.75	0.92	0.97	1.89

The fiber- matrix interface properties were achieved from fiber pullout tests on fibers treated with four different treatment processes. These interface properties were used to define the cohesive zone between polypropylene fiber and concrete matrix. Table 5.2 shows the interface properties for different treatment processes.

Table 5.2. Predicted cohesive zone parameters from single fiber pullout tests for different treatment cases.

Treatment Type	Maximum tangential traction (N)	Tangential displacement at maximum traction (mm)	Tangential displacement at the completion of debonding (mm)	
			Linear interpolation through peak and initial softening slope	Linear interpolation through peak and end failure point
Untreated fiber	0.162	0.15	0.3	6.4
Bromine treatment	1.07	0.2	0.4	5.5
Non-ionic detergent Treatment Type	0.84	0.2	1.3	5.6
PVAC treatment	1.52	0.275	1.1	5
Acid treatment	2.12	2.5	5.6	10.5

5.2.1. Response Optimization through Desirability Function

The desirability method is vastly used to determine the optimum conditions for process adjustment. The best possible scenario is met by optimizing multiple responses simultaneously. The method uses three different measures to reach the best condition, by maximizing, minimizing or by searching for nominal values of the condition specification. Desirability method is used to select the most feasible scenario for a particular process.

In this method, every single response (Y_1, Y_2...Y_k) of original set is transformed in a way so that d_i belongs to interval $0 \leq d_i \leq 1$. The d_i value increases when the ith response tends to approach the desired limits. Equation (1) is used to find the composite desirability, D, from combination of each responses processed through a geometric mean.

$$D = (d_1(Y_1) \times d_2(Y_2) \ldots \times d_k(Y_k))^{1/k} \quad (5.1)$$

The value D represents the level of combined responses based on the geometric mean calculated by equation 1. The index D also belongs to an interval of [0,1]. The value of D is maximized with all the responses approaching as close as possible to their specifications.

The closer the D is to 1 (one), the original responses will be closer to their individual specification limits. The geometric mean calculated from the individual desirability functions are maximized and then used to set the optimal point of the entire system. Wang et al. (2009) stated the advantages of using geometric mean. Geometric mean can be used to reach the final solution by allowing all the responses to reach to their desired values and then force the algorithm to approach the expected specifications.

According to Derringer et al. (1980), the algorithm will depend on the desired optimization type (maximization, minimization or normalization) within the specification and the weights of individual responses. The different optimization types are as follows:

a. Minimize Function: The desirability function value increases as the original response value approaches a minimum target value.

b. Normalize Function: When response moves toward the target, the desirability function value increases.

c. Maximize Function: The desirability function value increases when the response value increases.

In this study, the 'normalize function' type optimization is chosen. A target value is set for the responses, strength and stiffness, and the predictors are optimized to reach the target value. Fig. 5.1 shows the desirability function analysis technique to reach a target value.

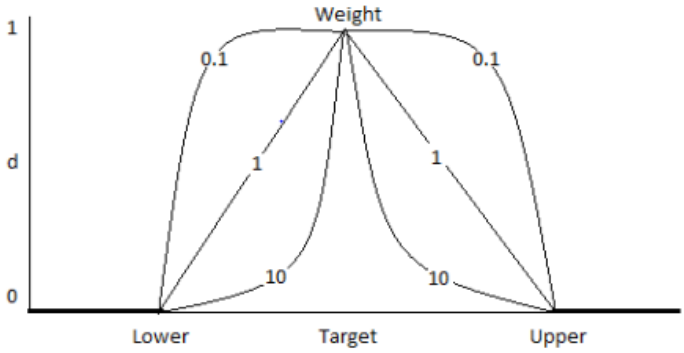

Fig. 5.1. Desirability function to hit a target value (Source: MINITAB reference)

The response and continuous predictors are taken as follows:

Responses:

1. Strength
2. Stiffness

Continuous Predictors:

1. Void percentage (15~20%)
2. Fiber percentage (1~3%)
3. Fiber-matrix interface properties
    a. Maximum traction
    b. Displacement at maximum traction
    c. Displacement at debonding

To perform a sample optimization, a target value for strength is set to 1.5 ksi and stiffness as 35 ksi. Five response variables have been selected to optimize the strength and stiffness so that the target value can be reached.

First a regression analysis is conducted to fit the model with the response and the variables. The correctness and the acceptability of the model are checked by the correlation coefficients R^2 and R^2 (adj). The regression analysis fits the model to the following equation:

Strength = 1.5523 - 0.03071 Void + 0.07222 Fiber + 0.0479 Max Traction

- 0.0118 Displacement at max traction + 0.0268 Displacement at debonding

For the Strength model, R^2 = 94.42 %, R^2 (adj) = 94.0 %.

Stiffness = 31.01 - 0.2152 Void + 0.8980 Fiber + 0.781 Max Traction

- 0.896 Displacement at max traction + 0.796 Displacement at debonding

For the Stiffness model, R^2 = 95.75 %, R^2 (adj) = 95.42 %.

The R-squared value test is performed to check if the variation in Y can be well explained by the regression model. R-squared value, also known as the co-efficient of determination, denotes how close the data are to the fitted regression line. The R-squared value for strength and stiffness analysis is 94.42% and 95.75% respectively, which indicates that 94.42% and 95.75% of the variation in Y can be explained by the regression model.

The diagnostic report illustrates the residuals vs the fitted values and any unusual points through the data can be identified (Fig. 5.2). The report shows that no residual data points exist based on the large residuals criteria, hence need no further investigation.

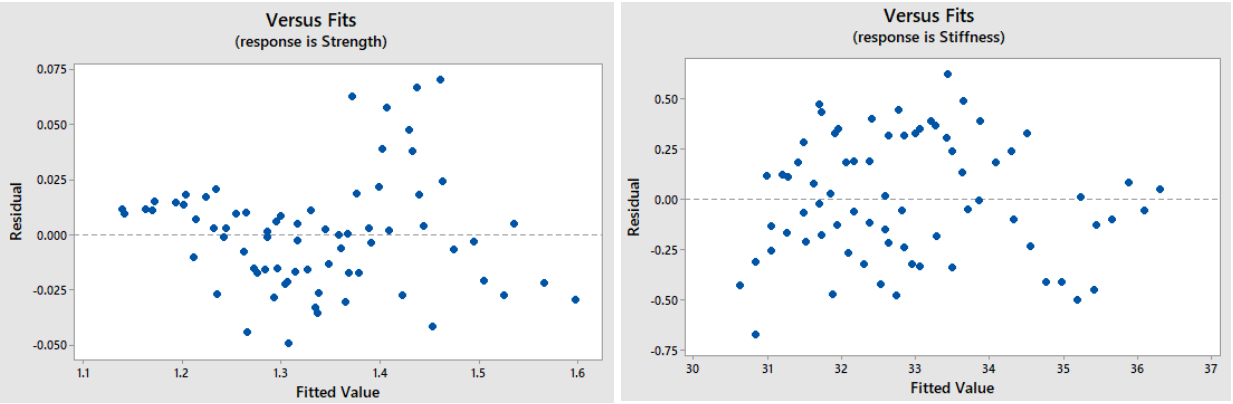

Fig. 5.2. Diagnostic report for unusual residuals

A good estimated regression model explains the variation of the dependent variable in the sample. Normal plots have the residuals being plotted versus their expected values when the

distribution is normal. Residuals are the difference between the observed and the fitted response value. The residuals from the analysis should be normally distributed.

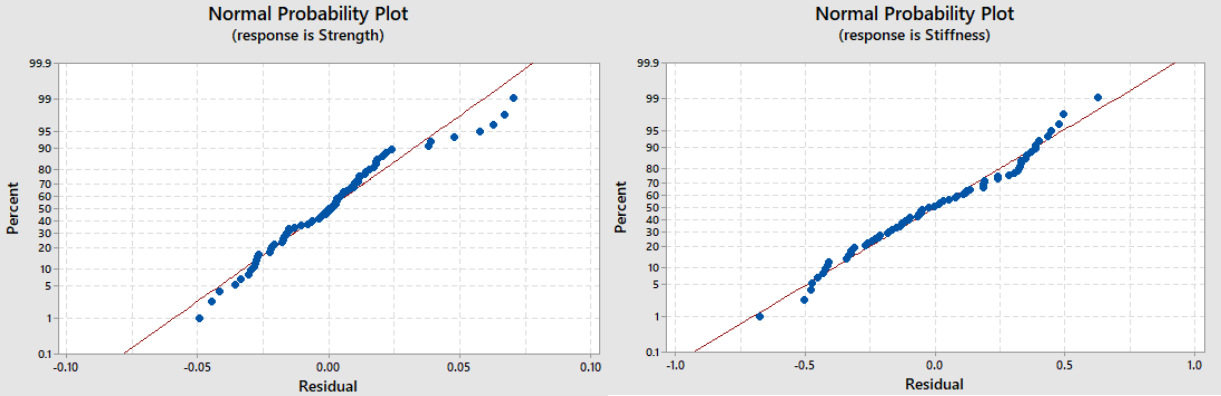

Fig. 5.3. Normal probability plot for strength and stiffness

From Fig. 5.3, it can be seen that the residuals are plotted around the straight line which indicates that the residuals are normally distributed. Hence, it can be said that the normality assumption is satisfied for both the responses (strength and stiffness) in this study. Therefore, there is no evidence of existance of nonnormality, skewness, outliers, or unidentified variables.

Then a P-value check was performed to validate the relationship between Y and X variables. This test is based on the level of risk (α) to conclude that a relationship exists between Y and X. The risk level α is set to be 0.001, and if the P-value falls below the risk level then the model can be taken as statistically significant.

The P-value check shows that $P<0.001$, in this case 0.0004, which denotes that the relationship between Y and the X variables in the model is statistically significant.

As the models fit the data well, the regression equations can be used to predict the optimized Strength and Stiffness (Y) for specific values of the X variables, or find the settings for the X variables that correspond to a desired value or range of values for Y.

Table 5.3 shows the target values of strength and stiffness along with their assigned weight and importance.

Table 5.3. Target parameters

Response Goal	Lower	Target	Upper	Weight	Importance
Stiffness Target	30.15	35.0	36.35	1	1
Strength Target	1.15	1.5	1.57	1	1

Based on the assigned target, the desirability function analysis is conducted using MINITAB response optimization tool. The method considers an objective function initially which transforms the existing values into a scale free value, desirability. Later composite desirability is evaluated based on which the optimum level of parameters is selected to reach the target strength and stiffness. Fig. 5.4 shows the prediction and optimization report generated in Minitab.

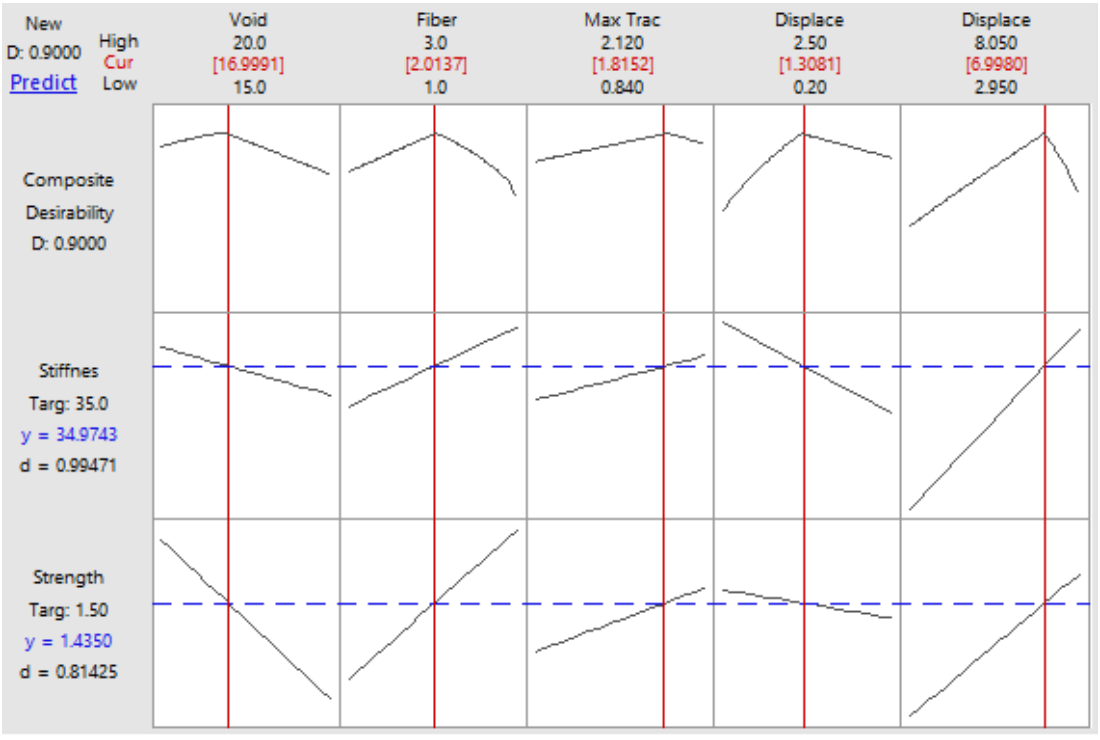

Fig. 5.4. Prediction and optimization report

Fig. 5.4 shows that the D value belonging to [0-1] interval, is maximized when all responses are close to their specifications. The closer D is of 1, the closer the original responses will be of their respective specification limits. The optimal general point of the system is the optimum point achieved by geometric mean maximization calculated from individual desirability functions (d). The individual desirability values for each one of response variables are: for stiffness, d = 0.99; for strength, d = 0.81.

The obtained value for composite desirability (D) shows that the process was well optimized to reach the target, since it is close (D=0.90) to the optimum condition (1.0). To reach this desirability, the continuous predictors are predicted and set as follows (Table 5.4):

Table 5.4. Multiple response prediction (target: strength 1.5 ksi and stiffness 35 ksi)

Variable	Setting
Void	17.00
Fiber	2.01
Max Traction	1.82
Displacement at max traction	1.31
Displacement at debonding	7.00

The predicted strength and stiffness for this optimization setting is 1.43 Ksi and 34.97 Ksi respectively, which falls within the range of 95% confidence interval and 95% prediction interval (Table 5.5).

Table 5.5. 95% confidence and prediction interval for strength and stiffness (strength 1.5 ksi, stiffness 35 ksi)

Response	Fit	95% CI	95% PI
Stiffness	35.00	(33.43, 36.58)	(33.31, 36.69)
Strength	1.50	(1.37, 1.63)	(1.36, 1.64)

A second optimization is then conducted by fixing the target value of strength and stiffness at 1.3 Ksi and 32 Ksi respectively. The individual desirability for strength and stiffness value is 0.995 and 0.977. The composite desirability is 0.986. The continuous predictors are set to reach the target is as follows (Table 5.6):

Table 5.6. Multiple response prediction (target: strength 1.3 ksi and stiffness 32 ksi)

Variable	Setting
Void	17.06
Fiber	2.00
Max Traction	1.09
Displacement at max traction	0.26
Displacement at debonding	2.95

The predicted strength and stiffness for this optimization setting is 1.30 Ksi and 32.10 Ksi respectively, which falls within the range of 95% confidence interval and 95% prediction interval (Table 5.7).

Table 5.7. 95% confidence and prediction interval for strength and stiffness (Strength 1.3 ksi, stiffness 32 ksi)

Response	Fit	95% CI	95% PI
Stiffness	32.00	(31.88, 32.32)	(31.44, 32.76)
Strength	1.30	(1.28, 1.32)	(1.25, 1.36)

5.2.2. Overlaid Contour Plot

Overlaid contour plots are used to visually identify the feasible variables for multiple responses in a model. Different responses may require different feasible variable settings. Applications involving multiple responses possess a challenge compared to single response studies. The optimal value of a response variable can significantly differ from the optimal value of another response. Overlaid contour plot allows to visually identify an area of compromise among the various responses.

Contour lines can be described as the curve that connects the data points in such a way that the fitted response values are equal. The region bounded by the contour lines defines the common region (if any) for all the responses within the upper and lower limits. The bounded region is known as the feasible region. The overlaid contour plot offers an envelope of the response variables, within which the response is feasible for a certain range of values.

In this study, overlaid contour plots have been generated to illustrate the effect of response variables (fiber, void percentages and interface properties) to the strength and stiffness of the polypropylene fiber reinforced pervious concrete.

The contour plots of the response with any two variables are generated to indicate the effect of those variables on the response within the fitted regression model. Each contour plot illustrates the significance of the two variables to optimize the response while the other variables are held to their mean values. Fig. 5.5 illustrates the contour plots for strength and stiffness.

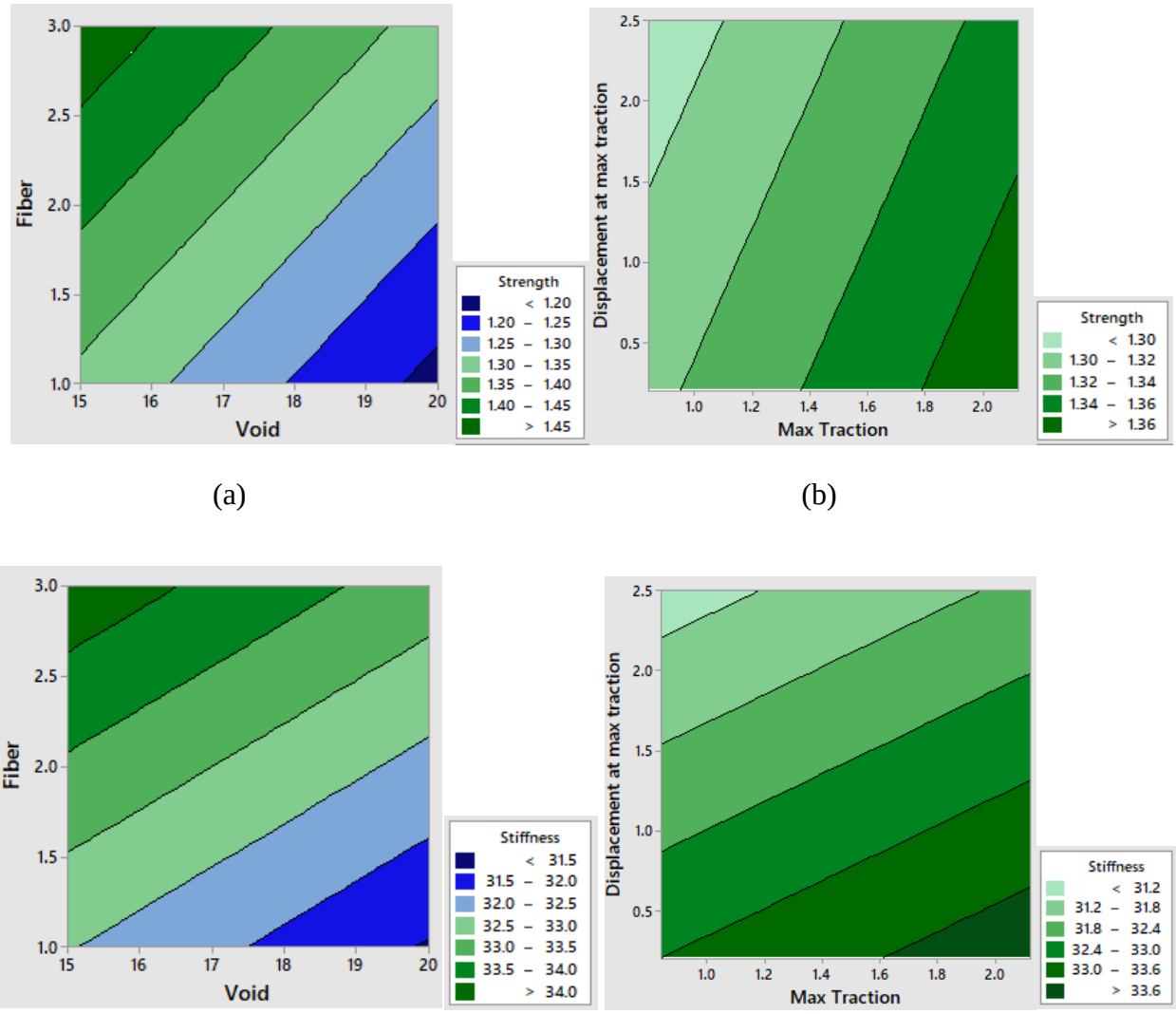

(a) (b)

(c) (d)

Fig. 5.5. Contour plots of (a)strength vs fiber, void, (b) strength vs maximum traction, displacement at maximum traction (c) stiffness vs fiber, void and (d) stiffness vs maximum traction, displacement at maximum traction

The individual contour plots were generated for each of the variables and then simultaneous optimization of properties were carried out by overlaying the individual plots to obtain the overlaid contour plot. The desired values of all these variables can be obtained at any given combination within the optimized region indicated by the white colored area on the overlaid contour plot.

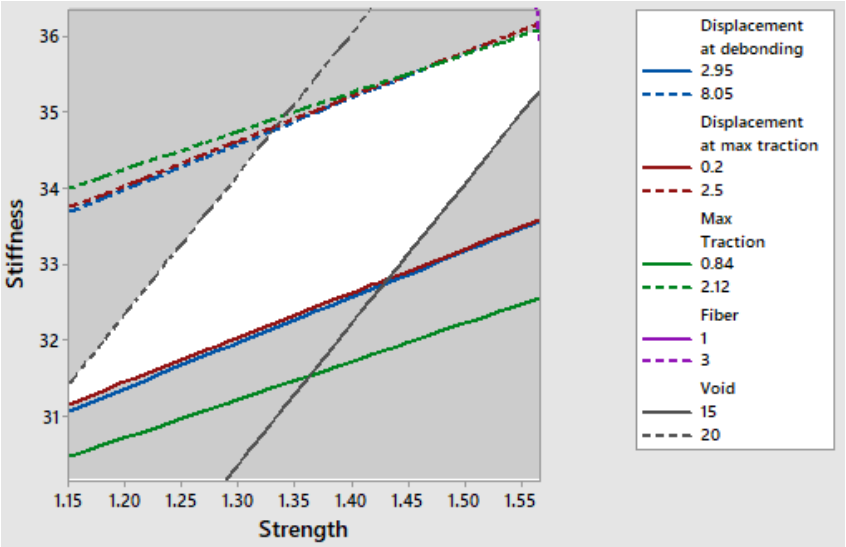

Fig. 5.6. Overlaid contour plot

Fig. 5.6 illustrates the overlaid contour plot considering the upper and lower bounds of continuous predictors. The white region is the feasible region to predict the strength and stiffness, satisfying the range of continuous variables.

5.3. Results and Discussion

Two optimization technique is adopted to optimize the strength and stiffness of fiber-reinforced pervious concrete matrix.

From the first method, composite desirability is set as the objective function. Two cases are studied to reach a target value for strength and stiffness. Both the cases reach to a composite desirability index close to optimum and optimizes the continuous predictors accordingly. This optimization method can be used to predict the required void and fiber percentages, as well as the required treatment method to reach a target strength and stiffness of the composite matrix.

From the first studied case (strength 1.5 Ksi and stiffness 35 Ksi), the interface parameters are optimized as: Void percentage = 17.00; Fiber percentage = 2.01; Maximum traction = 1.82 N; Displacement at maximum traction= 1.31 mm; Displacement at debonding= 7.00 mm.

Referring to Table 5.2, these interface property values can be reached with acid treatment of polypropylene fibers (Maximum traction = 2.12 N, displacement at maximum traction= 2.5 mm, displacement at debonding= 8.05 mm).

Similarly, from the second studied case (strength 1.3 Ksi and stiffness 32 Ksi), the interface parameters are optimized as: Void percentage = 17.06; Fiber percentage = 2.00; Maximum traction = 1.09 N; Displacement at maximum traction= 0.26 mm; Displacement at debonding= 2.95 mm.

Referring to Table 5.2, these interface property values can be reached with PVAC treatment of polypropylene fibers (Maximum traction = 1.52 N, displacement at maximum traction= 0.28 mm, displacement at debonding= 3.05 mm).

The second method of optimization, the overlaid contour plot illustrates an influence envelope for both the responses (strength and stiffness). The boundaries of acceptable values of the fitted response are defined by each set of contours. The lower bound is shown by the solid contour line, whereas the dotted contour line is used to define the upper bound. Different colors have been used to display the contours of each response.

5.4. Conclusion

The study discusses two optimization techniques to optimize the polypropylene fiber reinforced pervious concrete. The response optimization method allows to target a specific value of strength and stiffness based on the void ratio, fiber volume percentage, and interface properties database. The data extracted from ANSYS model is used to generate the regression equation and later the optimization technique is extended to reach to a desired value of strength and stiffness. The overlaid contour plot method can be used to illustrate the feasible zone of variables to reach to a specified strength and stiffness value. The optimization techniques are efficient and if the data is well distributed and offers significant relation among the variables, then the optimization can be

done within 95% confidence interval. However, optimization of fiber reinforced pervious concrete material requires more improvement and inclusion of other variables such as fiber size and shape distribution.

5.5. References

[1] Hashin Z., (1962). The elastic moduli of heterogeneous materials. J Appl Mech. 29: 143-150.

[2] Mori T., Tanaka K., (1973). Average stress in matrix and average elastic energy of materials with mis-fitting inclusions. Acta Metal 21: 571-583.

[3] Hill R., (1965). A self-consistent mechanics of composite materials. J. Mech. Phys. Solids 13: 213-222.

[4] Woo L.Y., Wansom S., (2005). Characterizing fiber dispersion in cement composites using AC-Impedance Spectroscopy. Cement and Concrete Composites 27(6): 627-636.

[5] Lee B.Y., Kim J.K., (2009). Quantitative evaluation technique of Polyvinyl Alcohol (PVA) fiber dispersion in engineered cementitious composites. Cement and Concrete Composites 31(6): 408-417.

[6] Yan Z., Yuexin D., (2009). The dispersion of SWCNTs treated by dispersing agents in glass fiber reinforced polymer composites. Composites Science and Tech. 69(13): 2115-2118.

[7] Ghasemi H., Brighenti R., Zhuang X., Muthu J., Rabczuk T., (2014). Optimization of fiber distribution in fiber reinforced composite by using NURBS functions. Computational Material Science 83: 463–473.

[8] Brighenti R., (2005). Fiber distribution optimization in fiber-reinforced composites by a genetic algorithm. Composite Structures 71: 1-15.

[9] Wang, J, Wan W., (2009). Application of desirability function based on neural network for optimizing biohydrogen production process, International journal of hydrogen energy, 34, 1253-1259.

[10] Derringer G., and Suich S., (1980). Simultaneous optimization of several response variables. Journal of Quantitative Technology 12(4): 214.

CHAPTER 6. CONCLUSIONS AND FUTURE WORK

6.1. Research Outcome

In this thesis, the research work is organized into four segments. The research objectives and methodologies are discussed through Chapter two to Chapter five. The findings from numerical simulations and laboratory experiments are compared and discussed elaborately in the previous Chapters. In this Chapter, the overall outcome of the research is summarized and the scope for future work on Fiber reinforced pervious concrete is suggested.

6.1.1. Image Based 2D Pervious Concrete Micromechanical Analysis

In the first segment of this study, pervious concrete microstructure has been studied through an image based micromechanical model. The scope of this study was to predict the behavior of pervious concrete through a representative volume element, consisting void and concrete phases. The 2D elastic model was generated in ANSYS with uniformly distributed voids. The uniform void distribution was justified through image analysis of pervious concrete specimen. However, in ANSYS generated 2D models, the voids were considered as circular in shape and not overlapping with each other. The stress-strain behavior of pervious concrete microstructure was compared with the stress-strain behavior obtained from laboratory experiments. Permeability, a very important property of pervious concrete was also studied through the 2D microstructure and laboratory experiments. The comparison between the properties of 2D microstructure and the real case scenario confirmed the validity of using the model as a representative volume element to study the pervious concrete further. The key findings of this segment are:

- Influence of the distribution of voids on strength, stiffness, and permeability of pervious concrete microstructure is studied by 2D image analysis and finite element modeling.

- The position and size distribution of the microstructure voids are summarized through Fast Fourier Transformation (FFT) analysis. A finite element analysis is conducted on the microstructure models regenerated through the derived microstructure characteristics using ANSYS Parametric Design Language (APDL).
- The effect of the sample size of 2D microstructures is studied by varying the section size and a possible representative volume element (RVE) is therefore found.
- Predicted stress-strain plots are generated for the 2D specimen under compressive loads and the obtained results, including stiffness, strength and permeability are compared with the results from the experiments conducted following ASTM standards.
- The comparison between models and physical experiments showed around or above 90% accuracy, which validates the suggested micromechanical analysis method of the previous concrete composite.

6.1.2. Chemically Treated Polypropylene Fiber as a Reinforcement in Pervious Concrete

This segment of the study discussed the applicability of chemically treated polypropylene fibers as a reinforcement in pervious concrete. As polypropylene fibers are inert and non-porous in nature, the focus of the chemical treatment was to enhance the roughness and porosity of the fibers so that the mechanical bonding between the fiber and the cement matrix was improved. The change of the polypropylene fiber surface was observed through a series of experiments which included fiber wettability test, fiber pullout test, and Atomic Force Microscopy (AFM). The treated fibers showed improved surface properties such as roughness and porosity. The single fiber pullout test results also confirmed a better bonding between the fiber and the matrix interface. The treated fibers are then used in pervious concrete to study the effect of chemical treatment on the fiber reinforced pervious concrete specimen. Though the compressive strength was not affected, flexural

strength of the fiber reinforced pervious concrete was significantly increased by the inclusion of chemically treated polypropylene fibers. The key findings of this segment of the study are:

- Chemically treated fibers have shown higher bond strength with the concrete matrix and largely increased the flexural strength than that of the control pervious concrete samples tested.
- Fiber reinforcement does not help improving the compressive strength of pervious concrete, which is mainly due to the flexible fiber type used in this study.
- Fiber-matrix interface behavior in pervious concrete determined through the fiber pullout test shows similar patterns as the fiber reinforcement in conventional concrete, including the linear loading region, the nonlinear-debonding region, the Fiber-matrix interfacial slip, and eventually cracking. However, verified with the experimental and numerical modeling, the affected zone of each fiber in pervious concrete is less compared to that of fiber reinforcement in conventional concrete, consistent with the St. Venant's principle.

6.1.3. 2D Fiber Reinforced Pervious Concrete Micromechanical Analysis

In the third segment of this study, a 2D fiber reinforced pervious concrete microstructure was generated based on the outcomes of the first two segments. The fibers were assumed to be elliptical and voids were kept as circular. Also, the voids were assumed not to be in contact with the fibers to avoid complex boundary conditions around the contact edges. To define the fiber-matrix interface, the mode II dominated bilinear cohesive zone model was adopted and the cohesive zone interface properties were extracted from single fiber pullout tests. The cohesive zone model was first verified through the force-extension behavior in experimental and simulated fiber pullout tests. The 2D fiber reinforced pervious concrete micromechanical analysis was then conducted under displacement-controlled loading to derive the strength and stiffness of the matrix.

A parametric study was conducted varying the void percentage (10%~15%), fiber percentage (1%~3%) and fiber-matrix interface properties obtained from four fiber treatment processes. The key findings of this segment of research are:

- Bilinear cohesive zone model is used to simulate the interface between fiber and concrete matrix. The comparison between the finite element model and the experimental results validates the definition of the model.
- A 2D microstructure of fiber reinforced pervious concrete is generated that consists of three phases: voids, fibers, and concrete matrix. The model is based on the outcome of the first segment of the study, which extends over the size of the representative volume element and includes realistic void distribution.
- A parametric study is conducted on the strength and stiffness of the composite matrix varying the voids, fibers and interface properties. The results from this parametric study give us a picture on how these variables affect the overall properties of fiber reinforced pervious concrete.

6.1.4. Possible Techniques to Optimize The Fiber Reinforced Pervious Concrete

In this final segment, two optimization techniques were applied to optimize the fiber reinforced pervious concrete for a specific strength and stiffness. The results from the parametric study conducted in the previous segment were utilized to optimize the strength and stiffness. The optimization techniques used were the desirability function method and the influence envelope method for multiple variables. The key findings of this segment are:

- The discussed optimization techniques can be used to optimize the strength and stiffness of fiber reinforced pervious concrete by suggesting the required void percentage, fiber percentage, and type of chemical treatment on polypropylene fibers.

- The optimization techniques can be used for multiple variables that affect the overall properties of fiber reinforced pervious concrete. The test cases presented in this segment consist of five variables, though more variables can be utilized to improve the accuracy of the optimized fiber reinforced matrix.

6.2. Future Work

Throughout this research, a 2D fiber reinforced pervious concrete micromechanical analysis is studied, which can be used as a representative volume element that shadows the properties of the entire specimen. However, the model can be improved to attain more accuracy by considering the variables that can affect the properties of fiber reinforced pervious concrete. The possible future work to overcome the deficiency of this research are described below.

- A 3D microstructure can be adopted to represent the pervious concrete matrix. Through the 3D microstructure, the crack propagation and void to void connectivity can be realistically designed.
- The visco-elastic properties of pervious concrete and polypropylene fibers can be studied to strengthen the understanding and assumptions of such matrices.
- Chemical analysis of the bonding zone between concrete matrix and polypropylene fibers can be considered to study if there is any significant chemical bonding.
- Fiber size and shape distribution can be added as variables that may affect the overall matrix properties. Considering these variables will certainly improve the accuracy of the microstructure model.
- Pervious concrete is vulnerable to freeze-thaw durability. The freeze-thaw durability study can be conducted with treated polypropylene reinforced pervious concrete specimen to ensure if it improves the overall matrix strength.

APPENDIX

Fig. A.1. (clockwise) Batch of fiber reinforced pervious concrete samples, void ratio test, compressive strength test, permeability test

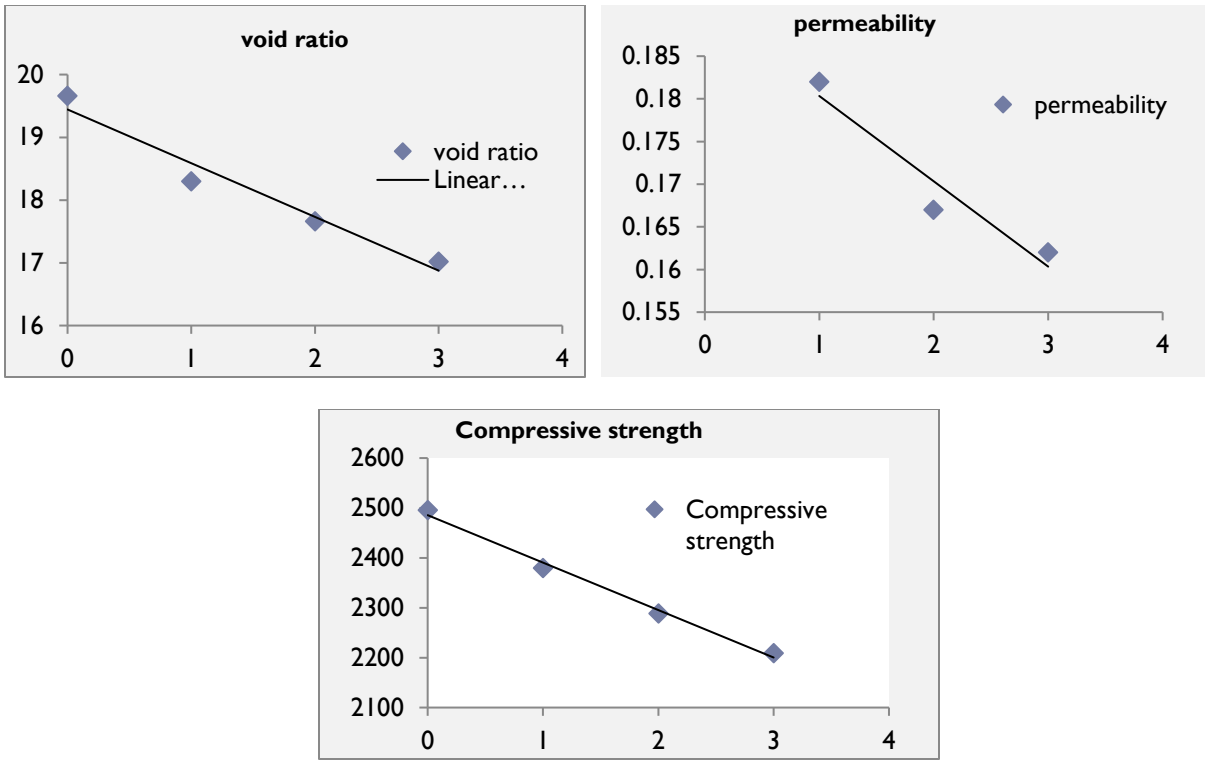

Fig. A.2. Properties of pervious concrete with inclusion of fiber (clockwise from top left), void ratio, permeability and compressive strength

Fig. A.3. MicroCT: GE vtomex s

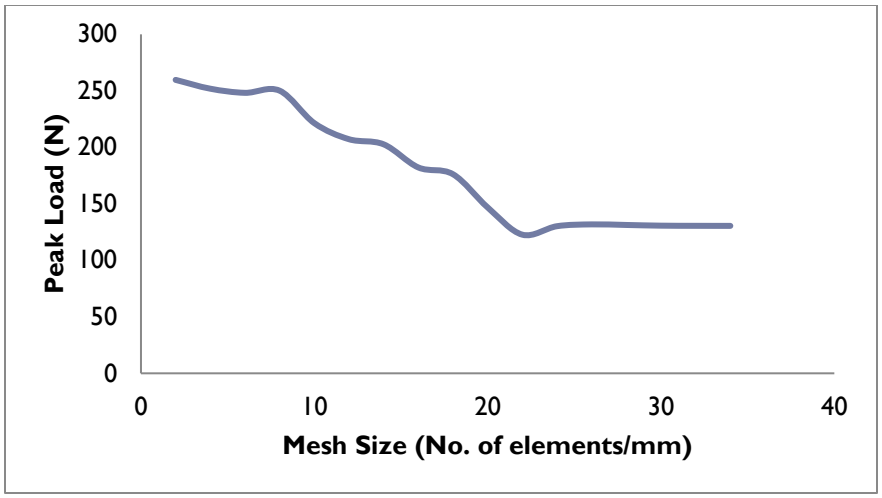

Fig. A.4. Mesh Sensitivity Study to select mesh size

Fig. A.5. Polypropylene fibers

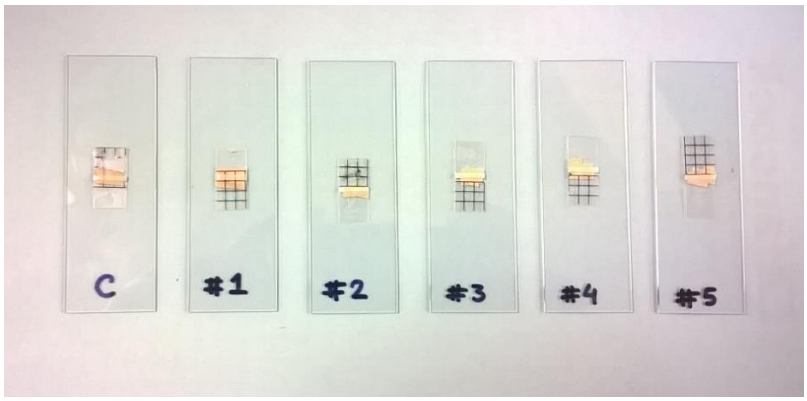

Fig. A.6. Prepared fiber specimen for AFM

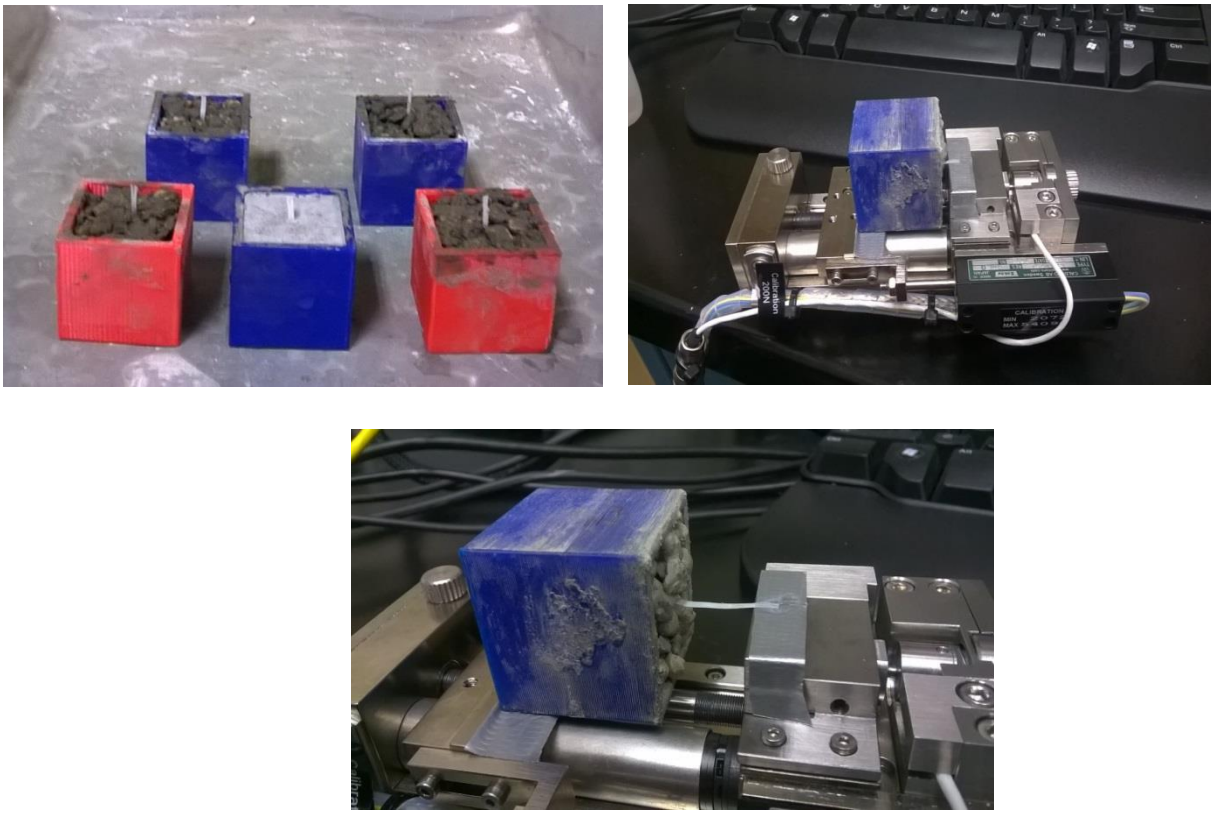

Fig. A.7. Fiber Pullout test setup (clockwise) specimen with single polypropylene fiber , pullout test setup, fiber pulled out from the matrix